frontiers in Materials

TYPE Original Research
PUBLISHED 31 July 2026
DOI 10.3389/fmats.2026.1800938

Check for updates

Constitutive structural response of Concrete Damaged Plasticity model under Willam's test

Diego Froio[1,2], Rosalba Ferrari[2] and Egidio Rizzi[2]*

[1]ISMES, Seriate (BG), Italy, [2]Dipartimento di Ingegneria e Scienze Applicate, Università degli studi di Bergamo, Dalmine (BG), Italy

OPEN ACCESS

EDITED BY
Giovanna Xotta,
University of Padua, Italy

REVIEWED BY
Xiaohu Yu,
The University of Melbourne, Australia
Nasser Alanazi,
University of Hail, Saudi Arabia

*CORRESPONDENCE
Egidio Rizzi,
egidio.rizzi@unibg.it

RECEIVED 31 January 2026
REVISED 16 February 2026
ACCEPTED 06 March 2026
PUBLISHED 31 July 2026

CITATION
Froio D, Ferrari R and Rizzi E (2026) Constitutive structural response of Concrete Damaged Plasticity model under Willam's test.
Front. Mater. 13:1800938.
doi: 10.3389/fmats.2026.1800938

COPYRIGHT
© 2026 Froio, Ferrari and Rizzi. This is an open-access article distributed under the terms of the Creative Commons Attribution License (CC BY). The use, distribution or reproduction in other forums is permitted, provided the original author(s) and the copyright owner(s) are credited and that the original publication in this journal is cited, in accordance with accepted academic practice. No use, distribution or reproduction is permitted which does not comply with these terms.

The present work aims to analyze and calibrate the mechanical description of plastic strain-induced anisotropy and damage coupling by the so-called Concrete Damaged Plasticity (CDP) constitutive model, which is rather well known, also since it has become available within popular FEM platforms, such as ABAQUS, and shall reproduce typical features of failure processes in quasi-brittle materials, such as concrete. This is achieved by combining an effective stress-based non-associative hardening/softening plasticity model with an isotropic damage model based on plastic strains, at a smeared continuum scale. In the paper, focusing on the mere elastoplastic coupling for tensile-dominated responses, and introducing an enhanced tuning by setting tensile exponential softening and damage evolutions through a convenient plastic to inelastic strain ratio parameter, by means of an external user implementation, an exhaustive numerical parametrization analysis is performed, starting at a constitutive-driver level, to experiment with the outcomes of the constitutive description and to quantify the amount of material anisotropy induced by plastic deformation, under biaxial elongation/shearing Willam's test, which prescribes/involves the rotation of the principal axes of strains/stresses. It is shown that the constitutive response is effectively regularized, allowing to fulfil the requirements of Willam's test, independently of the amount of inherent plastic dilatancy, showing a rather mild presence of plastic-induced anisotropy, at the pure constitutive-driver scale. Furthermore, first extrapolating implications and outcomes at the small (specimen) structural scale are also investigated, with clear appearance of strain localization and related much pronounced plastic-induced anisotropy, in the (imperfection-triggered) macroscopic response, with features that are similar to those coming, for example, from more sophisticated anisotropic damage models, while significant practical applications may subsequently follow, within different structural engineering contexts, such as that of large-scale concrete structures under static and dynamic loading scenarios, toward informed safety assessment and evaluation.

KEYWORDS
Concrete Damaged Plasticity (CDP) model, constitutive driver, plastic to inelastic strain ratio tuning, plastic-damage coupling, structural scale, Willam's test

1 Introduction

Currently, a reliable structural analysis of large-scale concrete structures, such as for instance reactor vessels, nuclear containments, offshore platforms, urban infrastructures and large dams, still constitutes a rather challenging task, within the field of structural engineering, including for possible validation, parameter calibration and model identification, which shall seemingly need to be supported by rather prohibitive experimental investigations, toward achieving a consistent digital twin replication, of the peculiar construction at hand, for informed management, maintenance, and safeguarding purposes.

Among that target, a main challenging feature is that of correctly describing the material range of constitutive response, especially within the inelastic range, as possibly linked to limit-state scenarios that may appear under non-conventional loading settings, and lead to nonlinear responses, even up to potential local or global failure, to be correctly described, by the inherent modelization, as focused on in the present investigation, as per the achievement of an appropriate and affordable description of the material model at hand.

In that, concrete indeed constitutes a strongly heterogeneous construction material, exhibiting several mutually interacting response mechanisms and features, including in the inelastic multi-dissipative range, such as different strength/stiffness under evolving tension/compression, anisotropic elastic degradation with microcrack growth, non-associated plastic flow, unstable post-failure behavior with strain localization phenomena, and hysteretic unloading loops, to mention a few principal characteristics. Therefore, the development of consistent and sufficiently accurate material response models for concrete at all stages of loading and ranges of stress-strain response reveals to be a rather demanding goal, including at an ideal smeared continuum scale, by the stipulation of appropriate constitutive models (material stress-strain laws).

Within such a continuum mechanics framework of macro/mesoscopic material behavior, it has widely been realized that multi-dissipative coupling between plasticity (permanent plastic strain dissipation) and damage (stiffness degradation dissipation) shall become fundamental, to effectively describe the nonlinear behavior of concrete materials (Bažant, 1980). Constitutive formulations of plasticity models for concrete shall also include a non-associated flow rule for the plastic strain rate and isotropic/kinematic hardening rules (Pramono and Willam, 1989), possibly accounting for softening, in the extended deformation range.

Even if a basic isotropic damage description of stiffness degradation may constitute a first, simplified behavioral assumption, for instance under mild damage conditions, isotropic damage models coupled with (isotropic) plasticity have shown acceptable capabilities of adequately describing concrete experimental responses under various nonproportional uniaxial and biaxial loading scenarios [e.g., (Grassl and Jirásek, 2006; Lee and Fenves, 1998; Lubliner et al., 1989; Xotta et al., 2016)].

Within that framework, the plastic-damage model by Lee and Fenves (1998), arising as an upgrade of the so-called "Barcelona model" by Lubliner et al. (1989), shall belong to this category [elastoplastic coupling, in the sense of Hueckel and Maier (1977), Maier and Hueckel (1979)]. The current availability of Lee and Fenves' constitutive plastic-damage model in the material library of popular commercial finite element program ABAQUS (2025), thereby with the rather well-known acronym of "Concrete Damaged Plasticity (CDP)" model, has seemingly boosted its widespread evaluation and adoption in both academic research investigations and engineering practice scenarios, aiming to achieve a consistent nonlinear structural analysis description of concrete materials and structures.

This holds true especially once involved expert users may want to go beyond mere "black-box" utilization, and possibly customize the capabilities of the inherent available constitutive model, at different structural response scales, to tailor and refine the computational tool to specific needs and response contexts. This calls for further inspection, understanding, and possible tuning, of consolidated features of the CDP model, to eventually formulate versatile and effective methods of structural analysis, response description, and interpretation.

Indeed, the CDP model shall describe in a rather affordable and efficient manner several of the fundamental features of the nonlinear mechanical behavior of concrete, such as: isotropic strength and stiffness degradation (strain-softening and damage) under tension, compression, tension-compression and shear stress-strain states; strength and ductility increase under compression at increasing lateral confinement; development of unrecoverable (plastic) strains after unloading; Microcracks Closing-Reopening (MCR) effects. However, no damage-induced anisotropy shall occur at the pure material point level, as investigated and confirmed in the present study. On the other hand, plastic strain-induced anisotropy shall take place, due to the intrinsic nature of the plastic part of the model, and this may be exacerbated by strain localization, at a "structural constitutive" specimen scale, as indeed shown in the current investigation. Therefore, a rigorous attempt to evaluate the amount of such anisotropy induction, as driven only by plastic processes, seems rather pertinent, to the expression of documented considerations about its influence on the overall CDP material response, and potentially relevant findings and implications at the structural scale.

This issue is tackled in the present paper, where systematic numerical experiments are performed for the CDP model, first at a mere constitutive-driver level, to evaluate the amount of rotation of principal stress directions, under prescribed rotation of principal strain directions, as dictated in the so-called biaxial extension/shearing Willam's test (Willam et al., 1987). Such a constitutive-driver test constitutes a rather intriguing scenario within which to inspect material model capabilities in multiaxial loading settings, leading to a potential anisotropic response, even starting from a virgin isotropic reference. Obviously, there also subsists an additional implicit, though evident, important reason to refer to the research work of K.J. Willam, and co-workers, as residing in the title and scope of the scheduled research project, to which the present paper attempts to contribute.

Beforehand, focusing on the sole elastoplastic coupling without MCR effects, and introducing into the CDP model an enhanced tuning by setting tensile exponential softening and damage curves through a convenient plastic to inelastic strain ratio parameter in the spirit of Ortiz (1985), by means of an external user implementation, an exhaustive numerical parametrization analysis of the CDP model is performed, starting at a constitutive-driver level, to experiment with the outcomes of the constitutive description and to quantify the (very small) amount of material anisotropy induced by homogeneous plastic deformation under Willam's test. It is shown that the constitutive response is effectively regularized, by the scheduled tuning refinement, allowing it to fulfill all requirements of Willam's test [specifically that of displaying no residual stresses at the end of the loading history in the presence of damage, see e.g., (Wosatko et al., 2020)], independently from the amount of inherent plastic dilatancy, showing a rather mild amount of plastic-induced anisotropy.

Then, first extrapolating implications and outcomes at the small (specimen) structural scale are also investigated, by FEM discretizations at the specimen size, with clear appearance of imperfection-triggered strain localization and related much pronounced damage- and plasticity-induced anisotropy, in the macroscopic response, showing features that interestingly arise rather similar to those from mechanical responses recorded, at the constitutive level, by more sophisticated anisotropic damage models [see (Carol et al., 2001a); (Carol et al., 2001b); (Carol et al., 2008)], such as resulting over-rotation of principal stresses with respect to ruling principal strains.

The presentation of the manuscript is organized as follows. The characteristic constitutive formulation of the CDP model is briefly summarized, in the various salient mathematical relations, in Section 2; there, the conditions under which anisotropic behavior may develop under general multiaxial stress states, including for biaxial Willam's test, are explored. The amount of plastic strain-induced anisotropy described by the CDP model at increasing values of inherent plastic dilatancy and cumulated plastic strains is effectively parametrized and discussed in detail in Section 3, where the outcomes of systematic numerical and parametric analyses performed at a constitutive-driver level within ABAQUS are presented, for a simulated biaxial Willam's test with a single and singly integrated finite element. Further implications, and response features, of planar Willam's test, at the structural constitutive scale of a specimen size, with imperfection-triggering of strain localization, and associated much visible plastic strain-induced anisotropy are then revealed in Section 4. Also, resuming specific and general considerations are eventually summarized in Section 5; this involves articulated parts and itemized lists, which are outlined to orientate the reader to the key facts of the analysis, and relevance about CDP model performance, specifically in the analyzed challenging context of multiaxial extension/shearing Willam's test, and to highlight specific and general significances of the present research investigation.

2 Concrete Damaged Plasticity (CDP) constitutive model

2.1 General constitutive relations

In the present section, the fundamental constitutive relations of the so-called rate-independent Concrete Damaged Plasticity (CDP) model for concrete are presented, within a standard small-strain framework. Index tensor notation is employed throughout, with Einstein's summation convention implied over repeated Latin indices, from 1 to 3. An overdot on top of variables marks a time derivative, i.e., the rate of a given quantity; since the considered constitutive model is rate-independent, such rates are linked to infinitesimal increments along a loading history, monitored by a monotonically growing parameter, say τ. A stress-state index $\iota \in \{t, c\}$ is adopted to distinguish between tensile-dominated (t) and compressive-dominated (c) stress-strain states, as it is meaningful to describe the different tension/compression response of concrete-like materials, as per the features of the CDP model.

The core state and rate constitutive relations governing the CDP material model may be summarized as follows (Grassl and Jirásek, 2006; Xotta et al., 2016):

$$\dot{\varepsilon}_{ij} = \dot{\varepsilon}^e_{ij} + \dot{\varepsilon}^p_{ij}; \tag{1a}$$

$$\dot{\sigma}_{ij} = (1-D)\dot{\bar{\sigma}}_{ij} - \dot{D}\bar{\sigma}_{ij}, \quad \dot{\bar{\sigma}}_{ij} = E^0_{ijkl}\dot{\varepsilon}^e_{kl}; \tag{1b}$$

$$1 - D = \left[1 - r\left(\bar{\sigma}_{ij}\right)D_t(\kappa_t)\right]\left(1 - D_c(\kappa_c)\right); \tag{1c}$$

$$\dot{\varepsilon}^p_{ij} = \dot{\lambda}\frac{\partial g\left(\bar{\sigma}_{ij}\right)}{\partial \bar{\sigma}_{ij}}; \tag{1d}$$

$$\kappa_t = \frac{1}{g^{pf}_t}\int_0^{\varepsilon^p_{I,M}} f_t(\kappa_t) r\left(\bar{\sigma}_{ij}\right) d\varepsilon^p_I,$$

$$\kappa_c = \frac{1}{g^{pf}_c}\int_{\varepsilon^p_{III,m}}^0 f_c(\kappa_c)\left[1 - r\left(\bar{\sigma}_{ij}\right)\right] d\varepsilon^p_{III};$$

$$\varepsilon^p_{I,M} = \max_t\left\{\varepsilon^p_I\right\}, \; \varepsilon^p_{III,m} = \min_t\left\{\varepsilon^p_{III}\right\}; \tag{1e}$$

$$\dot{\lambda} \geq 0, \quad \dot{f}\left(\bar{\sigma}_{ij}, \kappa_\iota\right) \leq 0, \quad \dot{\lambda}\dot{f}\left(\bar{\sigma}_{ij}, \kappa_\iota\right) = 0. \tag{1f}$$

Equation 1a expresses a traditional, small-strain, additive decomposition of strain rate tensor $\dot{\varepsilon}_{ij}$ into recoverable elastic ($\dot{\varepsilon}^e_{ij}$) and permanent plastic ($\dot{\varepsilon}^p_{ij}$) rate parts.

Equation 1b describes the rate form of the elastic stress-strain relation, where σ_{ij} and $\bar{\sigma}_{ij}$ are respectively the nominal and effective stress tensors, as being related to each other, implicitly through the principle of strain equivalence,

$$\sigma_{ij} = (1-D)\bar{\sigma}_{ij} \tag{2}$$

in terms of traditional scalar damage variable $0 \leq D \leq 1$, aimed at representing an isotropic elastic stiffness degradation, of current fourth-order secant elastic stiffness tensor $E_{ijkl} = (1-D)\,E^0_{ijkl}$, whereas

$$E^0_{ijkl} = \lambda_0\delta_{ij}\delta_{kl} + 2G_0\frac{1}{2}\left(\delta_{ik}\delta_{jl} + \delta_{il}\delta_{jk}\right);$$
$$\lambda_0 = \frac{\nu_0 E_0}{(1+\nu_0)(1-2\nu_0)},$$
$$G_0 = \frac{E_0}{2(1+\nu_0)}; \tag{3}$$

is the fourth-order initial isotropic elastic stiffness tensor, i.e., that of the intact (undamaged) material, depending on classical Lamé's constants λ_0, G_0 (E_0: Young's modulus, ν_0: Poisson's ratio), and δ_{ij} are Kronecker's delta components of second-order identity tensor $I_{ij} = \delta_{ij}$. The fourth-order initial isotropic elastic compliance tensor is further denoted as $C^0_{ijkl} = E^{0\;-1}_{ijkl}$.

Equation 1c for the $(1-D)$ term expresses the proposal of Lee and Fenves (Grassl and Jirásek, 2006), which potentially describes MCR effects, through two inherent damage variables, to account for damage states due to prevailing tensile (D_t) and compressive stress-strain states (D_c), and by an isotropic weight function, $0 \le r \le 1$, of effective stress tensor $\bar{\sigma}_{ij}$, related to a stiffness recovery effect:

$$r(\bar{\sigma}_{ij}) = \begin{cases} 0 & \text{if } \bar{\sigma}_{ij} = 0 \\ \dfrac{\sum_{K=1}^{3} \langle \bar{\sigma}_K \rangle}{\sum_{K=1}^{3} |\bar{\sigma}_K|} & \text{otherwise} \end{cases}; \tag{4}$$

where $\langle \cdot \rangle$ denotes the McAulay bracket operator (i.e., the positive part or ramp function) and $\bar{\sigma}_K$ $(K = 1,2,3)$ are the principal stresses related to the effective stress tensor.

Equation 1d expresses a non-associative flow rule, for plastic strain rate $\dot{\varepsilon}^p_{ij}$, as per the gradient of a plastic-potential scalar function $g(\bar{\sigma}_{ij})$ of the effective stress, magnified by non-negative single plastic multiplier $\dot{\lambda}$. Since the inherent Drucker-Prager (DP) plastic-potential function of the original Lee and Fenves' CDP model displays a singular point at the apex of the DP cone, which may be rounded for a convenient numerical treatment, the following DP hyperbolic function has been made available within the ABAQUS implementation (ABAQUS, 2025):

$$g(\bar{\sigma}_{ij}) = \sqrt{(\alpha'_d f_{t0} e)^2 + 3\bar{J}_2} - \frac{1}{3}\alpha'_d \bar{I}_1 \tag{5}$$

where $\bar{I}_1 = \mathrm{tr}(\bar{\sigma}_{ij}) = \bar{\sigma}_{ii}$ is the first invariant of the effective stress tensor, $\bar{J}_2 = \bar{s}_{ij}\bar{s}_{ij}/2$ is the second invariant of the deviator of the effective stress tensor, $\bar{s}_{ij} = \bar{\sigma}_{ij} - \bar{I}_1/3\delta_{ij}$, f_{t0} is the uniaxial tensile failure stress of the undamaged material, α'_d is the dilatancy factor inherent in the definition of g by Equation 5, linked to dilatancy angle ψ'_d as $\alpha'_d = \tan \psi'_d$ in (Xotta et al., 2016), while parameter e, named eccentricity, controls the function rate in approaching its asymptotic trend (tending to a straight line in the $\bar{p}$-$\bar{q}$ plane, as $e \to 0$, where $\bar{p} = \bar{I}_1/3$ and $\bar{q} = \sqrt{3\bar{J}_2}$).

Equation 1e characterizes the hardening/softening rules for the evolution of two independent normalized internal variables $0 \le \kappa_\iota \le 1$ $(\iota \in \{t, c\})$, namely the non-decreasing hardening variables of classical plasticity, once plastic deformation occurs (Oller et al., 1990). The limit value of $\kappa_\iota = 1$ denotes the complete loss of cohesion of the material point. This may be interpreted as the formation of a macroscopic crack. Hardening variables κ_ι are employed to express the evolution of tensile/compressive strengths $f_t(\kappa_t), f_c(\kappa_c)$ and different damage states $D_t(\kappa_t), D_c(\kappa_c)$ under tensile/compressive loading. Then, four material functions, f_t, f_c, D_t, D_c, either expressed in terms of κ_t, κ_c or directly in terms of maximum and minimum principal plastic strains $\varepsilon^p_I, \varepsilon^p_{III}$, must be specified, as input data, for the given material description to be reproduced for the implemented CDP constitutive model.

In Equation 1e, quantities g^{pf}_t and g^{pf}_c label the dissipated energy densities by plastic deformation, i.e., the areas underneath the stress-plastic strain curves in uniaxial tension and compression (Grassl and Jirásek, 2006), respectively:

$$g^{pf}_t = \int_0^{+\infty} f_t \, d\varepsilon^p_t \; (\varepsilon^p_t = \varepsilon^p_I), \quad g^{pf}_c = \int_0^{+\infty} f_c \, d\varepsilon^p_c \; (\varepsilon^p_c = -\varepsilon^p_{III}). \tag{6}$$

In the CDP model, such plasticity-driven dissipated energy densities may be linked with specific fracture energies g^f_t and g^f_c (energy per unit volume, i.e $[\mathrm{F}]/[\mathrm{L}]^2$), i.e., the total dissipated energies along the entire tensile and compressive inelastic processes (plasticity plus ensuing elastic stiffness degradation or damage), as described in Section 2.2.

Equation 1f expresses the often-named Kuhn-Tucker (compatibility) conditions representing the loading/unloading criterion at the current yield limit ($f = 0$), whereby isotropic yield/failure or loading function f, which limits the current admissible stress states ($f \le 0, \dot{\lambda} f = 0$) and evolves with the loading process, takes the following modified DP-like form (Oller et al., 1990):

$$f(\bar{\sigma}_{ij}, \kappa_\iota) = \frac{1}{1-\alpha}\left[\sqrt{3\bar{J}_2} + \alpha \bar{I}_1 + \beta(\kappa_\iota)\bar{\sigma}_I\right] - \bar{f}_c(\kappa_c) \tag{7}$$

where dimensionless coefficient

$$\beta(\kappa_\iota) = \begin{cases} (1-\alpha)\dfrac{\bar{f}_c(\kappa_c)}{\bar{f}_t(\kappa_t)} - (1+\alpha) & \bar{\sigma}_I \ge 0 \\ \gamma & \bar{\sigma}_I \le 0 \end{cases}; \tag{8}$$

evolves along the loading history, while $\bar{f}_t = f_t/(1 - D_t)$ and $\bar{f}_c = f_c/(1 - D_c)$ are respectively the tensile and compressive strengths of the intact material, whereas α, γ are two characteristic parameters affecting the shape of loading function f.

In short, the (driving) plastic part of Lee-Fenves' CDP model is based on the effective stress space and is defined by a specific yield function, a non-associated flow rule, evolution laws for the hardening variables, and loading-unloading conditions. Instead, stiffness degradation by damage is directly prescribed by cumulated plastic deformation through imposed material functions $D_t(\kappa_t)$ and $D_c(\kappa_c)$. This importantly implies that, in the CDP model, stiffness degradation cannot occur independently from plastic deformation [single-dissipative material, Rizzi et al. (1996)], as also assumed in other concrete-like constitutive models [e.g., (Meschke et al., 1998)]. Thus, the proper framework for setting the material description by the CDP model is that of "elastoplastic coupling" [(Hueckel and Maier, 1977; Maier and Hueckel, 1979)].

2.2 Energy densities and objectivity of the CDP material response

The governing equations of the CDP model depend on total dissipated energy densities by plastic deformation g^{pf}_ι [Equation 1e], as discussed in Section 2.1. Unfortunately, such energy densities cannot directly be extracted from experimental stress-strain diagrams. Rather, total dissipated energies along the entire tensile and compressive inelastic processes may be obtained as the corresponding areas under the uniaxial stress-strain diagrams:

$$g^f_t = \int_0^{+\infty} f_t(\kappa_t) d\varepsilon^i_I, \quad g^f_c = \int_{-\infty}^{0} f_c(\kappa_c) d\varepsilon^i_{III}; \tag{9}$$

where ε^i_I and ε^i_{III} are the maximum and minimum principal values of the total irrecoverable inelastic strain tensor:

$$\varepsilon^i_{ij} = \varepsilon^p_{ij} + \varepsilon^{ed}_{ij} = \varepsilon_{ij} - \varepsilon^{e0}_{ij}; \tag{10}$$

as given by the sum of the plastic strain tensor ε^p_{ij} and the overall deformation driven by elastic stiffness degradation:

$$\varepsilon^{ed}_{ij} = \frac{D}{1-D} C^0_{ijkl}\sigma_{kl}. \tag{11}$$

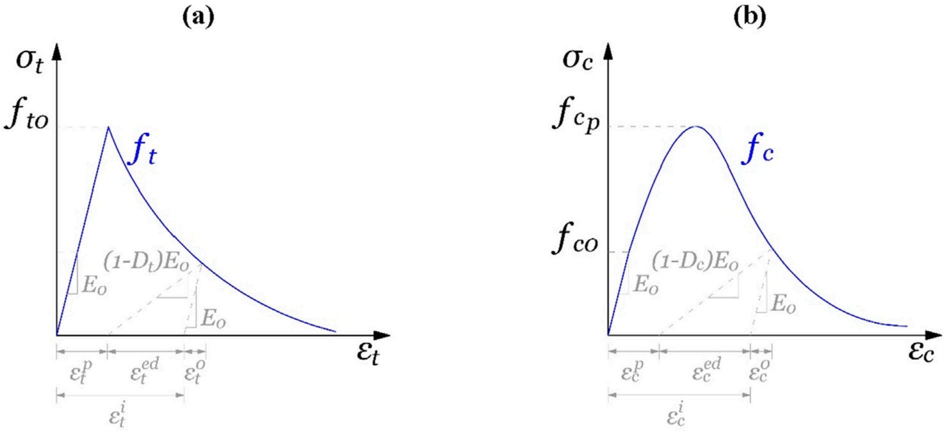

FIGURE 1
Uniaxial response curve of the CDP material model, **(a)** in tension and **(b)** in compression.

In other words, ε_{ij}^i is the current total strain tensor minus the elastic strain tensor (ε_{ij}^{e0}) that would elastically be recovered with the initial undamaged elastic stiffness, E_{ijkl}^0 (or compliance C_{ijkl}^0).

Under uniaxial monotonic loading conditions (see Figure 1), differentiation of Equation 10:

$$d\varepsilon_\iota^p = d\varepsilon_\iota - d\varepsilon_\iota^0 - d\varepsilon_\iota^{ed} = d\varepsilon_\iota - \frac{1}{E_0}\left[df_\iota + \frac{f_\iota}{(1-D_\iota)^2}dD_\iota\right]$$
$$= d\varepsilon_\iota - \frac{1}{E_0}\left[f_\iota'(\kappa_\iota) + \frac{f_\iota(\kappa_\iota)D_\iota'(\kappa_\iota)}{(1-D_\iota(\kappa_\iota))^2}\right]d\kappa_\iota; \qquad (12)$$

allows one to obtain the plastic strain increments in terms of four material functions f_ι, D_ι ($\iota \in \{t,c\}$) and total strain ε_ι, where the prime denotes differentiation with respect to the indicated argument. Then, substitution of Equation 12 into the integrals of Equation 6 allows one to numerically compute g_ι^{pf} from quantities that are directly obtained from experimental stress-strain diagrams. Accordingly, the sought relationship between total dissipated energy densities by plastic deformation g_ι^{pf} and total fracture energy density g_ι^f is obtained by substituting Equations 9 and 12 into Equation 6:

$$g_\iota^{pf} = g_\iota^f - \frac{1}{E_0}\int_0^1 \bar{f}_\iota^2(\kappa_t)D_\iota'(\kappa_t)d\kappa_t, \quad \iota \in \{t,c\}. \qquad (13)$$

It has been made abundantly clear over the past decades that the strain-softening branch of the stress-strain curves does not represent a local physical property of the material. The arguments have been advanced both on physical grounds and on the basis of the mesh sensitivity of numerical FEM solutions. Thus, dissipated energy densities g_ι^f ($\iota \in \{t,c\}$) should depend on the size of the strain localization zone, at the structural scale, possibly also through the adopted discretization size, at the FEM level, to warrant the overall objectivity of the underlying "local" material description within the global resulting softening regime. Since the inherent capacity for the dissipated energies per unit volume is not a material property, g_ι^f ($\iota = t,c$) should be derived from other recordable material properties, such as the fracture energies.

Assuming that the fracture energy in uniaxial tension (G_t^f) and its counterpart in uniaxial compression (G_c^f), with dimensions of [F]/[L], shall be interpreted as inherent material properties, each specific energy density g_ι^f shall be equal to the corresponding fracture energy normalized by the size of a localization zone, namely, a material characteristic length h_ι^{ch}, or crack band width (Bažant and Oh, 1983), leading to $g_\iota^f = G_\iota^f/h_\iota^{ch}$.

In FEM analysis, the material characteristic lengths may be linked to the finite element characteristic length, l^e, to achieve a fracture-energy-based regularization, by the use of a standard "local model" (such as the CDP one). This approach largely eliminates the mesh sensitivity of numerical solutions obtained by the FEM. The value of h_ι^{ch} is immaterial for the analyses performed at the material point level (Section 3) and, thus, h_ι^{ch} is arbitrarily set equal to unity in the present investigation. Instead, the fracture-energy-based regularization ($h_\iota^{ch} = h^e$) has consistently been enforced in the simulations focused on the description of the structural constitutive scale (Section 4).

The CDP model is a well-documented one, within the dedicated literature, and in FEM user manuals. Figure 1 however condenses the salient illustration of main key ingredients of the model, in terms of description of inherent inelastic effects, as per the interpretation and tuning that is then proposed within the paper.

The present discussion refers to a rate-independent description of inelastic material behavior under standard quasi-static scenarios. Further generalized material descriptions in the context of the dynamic behavior of concrete may be found in Grassl et al. (2011), Grassl et al. (2013), and specifically under impact loading in Yu et al. (2025a), Yu et al. (2025b).

2.3 Plastic strain-induced anisotropy of the CDP constitutive model

In the undamaged state, the concrete material is taken to display an isotropic and linear elastic behavior, whereby the corresponding fourth-order elastic stiffness tensor is provided by Equation 3. After inelastic phenomena (linked to driving plastic deformation, and attached stiffness degradation) have taken place, either in tension or in compression, the material response is ruled by the following constitutive law, among nominal stress and elastic strain tensors:

$$\sigma_{ij} = (1-D)E^0_{ijkl}\varepsilon^e_{kl} = \left[1 - r\left(\overline{\sigma}_{ij}\right)D_t\right](1-D_c)E^0_{ijkl}\varepsilon^e_{kl}. \tag{14}$$

Moreover, the spectral representations of elastic strain and effective stress tensors, in their (common) principal directions $\hat{e}^K_i$,

$$\varepsilon^e_{ij} = \sum_{K=1}^{3} \varepsilon^e_K \hat{e}^K_i \hat{e}^K_j; \tag{15a}$$

$$\overline{\sigma}_{ij} = \sum_{K=1}^{3} \overline{\sigma}_K \hat{e}^K_i \hat{e}^K_j, \quad \overline{\sigma}_K = \lambda_0 \varepsilon^e_{ii} + 2G_0\varepsilon^e_K; \tag{15b}$$

show that $\overline{\sigma}_{ij}$ and ε^e_{ij} are inherently coaxial, due to the isotropic nature of the material behavior, i.e., of E^0_{ijkl}. Substitution of Equations 15a,b into Equation 14 brings to the following analogous spectral decomposition of the nominal stress tensor:

$$\sigma_{ij} = \sum_{K=1}^{3} \left[1 - \hat{r}\left(\varepsilon^e_{ij}\right)D_t\right](1-D_c)\overline{\sigma}_K \hat{e}^K_i \hat{e}^K_j; \tag{16}$$

where

$$\hat{r}\left(\varepsilon^e_{ij}\right) = \begin{cases} 0 & \text{if } \varepsilon^e_{ij} = 0 \\ \dfrac{\sum_{K=1}^{3}\langle \lambda_0\varepsilon^e_{ii} + 2G_0\varepsilon^e_K\rangle}{\sum_{K=1}^{3}|\lambda_0\varepsilon^e_{ii} + 2G_0\varepsilon^e_K|} & \text{otherwise} \end{cases}; \tag{17}$$

is weight function r, hereby expressed in terms of the principal values of the elastic strain tensor.

Equation 16 shows that the principal values of nominal stress σ_{ij} turn out piecewise-smooth invariant functions of the principal values of elastic strain ε^e_{ij}. Then, according to a known theorem for elastic (or Cauchy elastic) materials (Ogden, 1997), the nominal stress turns out to be an isotropic function of the elastic strain. Hence, σ_{ij} is anyway coaxial to ε^e_{ij}, like $\overline{\sigma}_{ij}$. Then, no strain-induced anisotropy linked to damage could be recorded, in contrast with the response that may be recorded from smeared crack models (Willam et al., 1987). Therefore, in the constitutive response of the CDP model, ruled by Equations 1–17, plasticity-driven isotropic stiffness degradation of the classical $(1-D)$-type cannot induce, *per se*, any anisotropy in the material description. In other words, when plastic deformation processes remain negligible, i.e., when total strains are dominated by elastic strains, i.e., once $\varepsilon_{ij} \cong \varepsilon^e_{ij}$, the modeled quasi-brittle material behavior remains isotropic.

The only source of strain-induced anisotropy inherent to the CDP model at the material point level is related to the development of plastic strains, tied to the plastic part of the elastoplastic coupling within the model, which is ruled by effective stress path and dilatancy. These considerations, from the theoretical formulation of the constitutive model, are going to be confirmed by extensive numerical simulations of Willam's test, at the pure constitutive-driver level, developed in ensuing Section 3. On the other hand, one may notice that the inherent local isotropy of the CDP secant stiffness affected by stiffness degradation, driven by plastic strains, should not be conceived as a total limitation, in that global anisotropy to be experienced at the structural scale, due to localized deformation/cracking, may still locally be represented through an isotropic model. In fact, the ensemble response of the crack, i.e., the geometrical locus of isotropically damaged elements (Oliver et al., 1990), and the surrounding intact material, i.e., the geometrical locus of elements undergoing elastic unloading, may provide the sought-after anisotropic behavior. This is going to be shown, and discussed, with subsequent simulations at the structural scale, as further produced in Section 4.

3 Constitutive response of the CDP model to biaxial Willam's test

In the present section, the tensile-dominated response of concrete-like materials under prescribed rotation of the principal axes of strain, as predicted by the CDP constitutive model, is numerically evaluated by a constitutive driver, with the goal of observing its resulting performance in terms of plastic strain-induced anisotropy. Then, assuming a homogeneous deformation field, the constitutive response within an ideal two-dimensional concrete specimen is investigated as a numerical experiment at the material point level.

Reference is thus made to a single planar square four-node finite element, with a single Gauss integration point, under plane-stress conditions (namely, with no confinement in the out-of-plane direction). The single finite element (as per a single material point) is subjected to a specific nonproportional, strain-driven biaxial loading path with rotating principal directions of strains, through elongation and shearing, as per the so-called and rather well-known biaxial Willam's test, originally conceived by Willam et al. (1987), to assess and compare the material representations of fixed vs. rotating crack models with plastic softening models. This numerical test has acquired high visibility and has become widely used to verify and compare the outcomes of constitutive models for cracking and damage in quasi-brittle materials, such as geomaterials, concrete, masonry, and so on (Carol et al., 2008).

The two strain-driven phases characterizing biaxial Willam's test (Willam et al., 1987) of combined extension and shearing, schematically depicted in Figure 2, may be defined as follows:

- Initially, the virgin continuum is subjected to tensile straining (elongation), in the x_1-direction, within the elastic isotropic range, thus accompanied by a transverse Poisson's contraction in the x_2-direction, i.e., with strain rates in ratios $\dot{\varepsilon}_{11}:\dot{\varepsilon}_{22}:2\dot{\varepsilon}_{12} = 1:-\nu_0:0$, up to first cracking in uniaxial tension/extension.
- Immediately after cracking initiation, a sudden switch is made to combined biaxial extension and shearing deformation, according to scheduled strain rate ratios $\dot{\varepsilon}_{11}:\dot{\varepsilon}_{22}:2\dot{\varepsilon}_{12} = 0.5:0.75:1$, as further suggested in (Rots, 1988) and subsequently adopted in the dedicated literature, e.g., in (Wosatko et al., 2020; Carol et al., 2001b; Meschke et al., 1998; Oliver et al., 1990; Guzina et al., 1995). Such an imposed subsequent straining path forces a continuous rotation of the local principal directions of strain after crack nucleation, as later displayed in the model outcomes. The resulting strain rotation rate is faster, at the beginning of the numerical test, and progressively slower, later on, along the softening range with progressive material disruption, with a final asymptotic rotation value that comes from the imposed

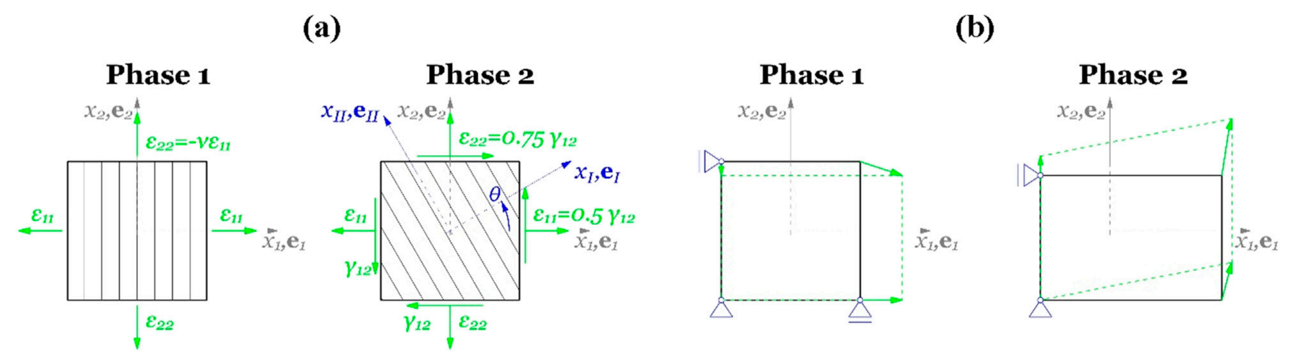

FIGURE 2
Biaxial Willam's test: **(a)** layout of combined tension-shear model problem and **(b)** prescribed element displacements for the corresponding strain state.

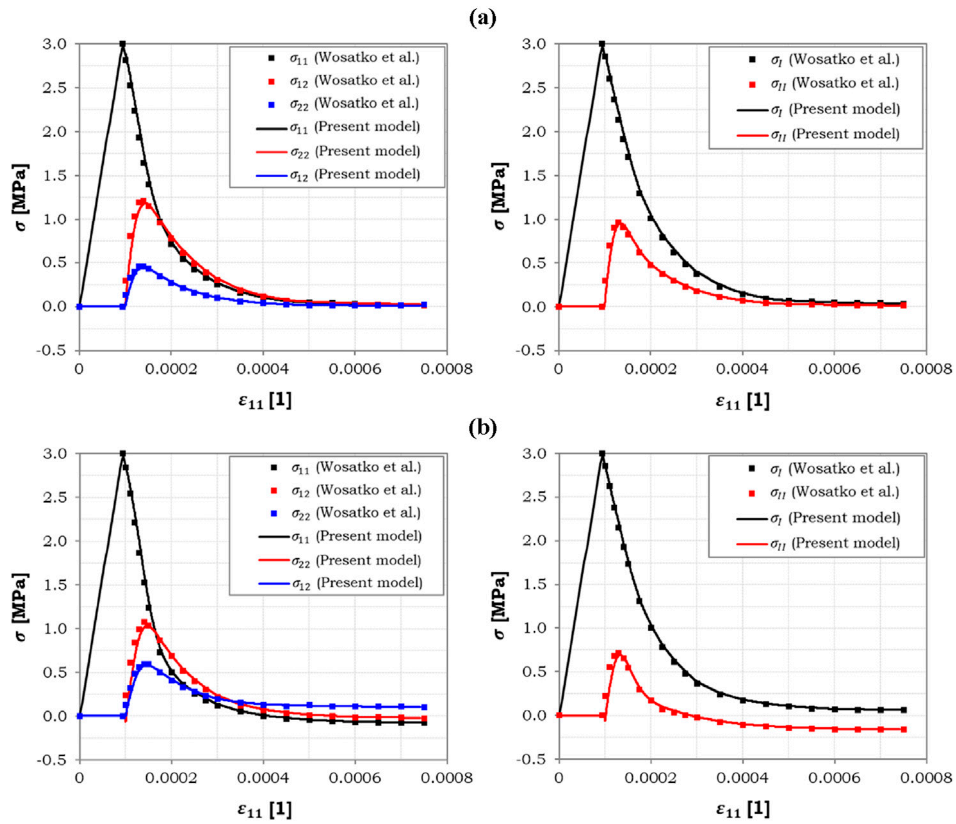

FIGURE 3
Comparison of stress components obtained from Willam's test with those reported by Wosatko et al. (2020): **(a)** elastoplasticity coupled with damage ($\psi_d' = 25°$, $D_t\left(\varepsilon_I^i\right) \neq 0$) and **(b)** pure elastoplastic behavior ($\psi_d' = 55°$, $D_t\left(\varepsilon_I^i\right) = 0$); first column: Cartesian stress components; second column: principal stress components.

strain ratios to about $\theta_{\text{lim}} = 90° - 1/2\,\text{atan}[1/(0.75 - 0.50)] \cong 52.02°$, from classical Mohr's circle analysis, of the strain rate tensor [see e.g., illustrations in Figure 1 of (Wosatko et al., 2020)].

The numerical constitutive analysis (quasi-static implicit time integration at the single Gauss point level), performed within the ABAQUS platform (ABAQUS, 2025), requires pertinent small strain increments, to minimize arising computational errors. During the second phase of Willam's test, the maximum allowed normal strain increment is set equal to 10^{-3} of its final value. Therein, the backward Euler scheme is employed, to resolve the constitutive response for the resulting stress history under imposed strain increments, for Willam's test combined extension/shearing deformation path.

TABLE 1 **Flowchart of the proposed external parametrization of the tensile part of the CDP model.**

Steps	Operations
1	Select basic free tensile softening material parameters f_{t0} and g_t^f, to evaluate $\varepsilon_t^{ch} = g_t^f / f_{t0}$ (or directly set ε_t^{ch}, leading to a value of specific fracture energy g_t^f at desired uniaxial tensile strength f_{t0}, also linked to Young's modulus E_0 or peak normal strain $\varepsilon_{t0} = f_{t0}/E_0$, for the virgin elastic material).
2	Depict the tensile exponential softening description in Equation 18, if adequate for the specific behavior at hand, and perforate it to appropriate numerical values (with a sufficient resolution), to be set as input as a first numerical tensile material function within the FEM code.
3	Set plastic to inelastic strain ratio parameter $0 < \alpha_p \leq 1$, tuning the amount of elastoplastic coupling (tending to 0 for negligible plasticity, to 1 for negligible damage).
4	Depict the tensile damage description in Equation 23, if adequate for the specific behavior at hand, and perforate it to appropriate numerical values (with a sufficient resolution), to be set as input as a second numerical material function within the FEM code.
5	Convey data of tensile softening strength and damage curves as input platform data (e.g., into an ABAQUS input file or CAE environment).

3.1 Validation of the implemented Willam's test

With the goals of inquiring into the consistency of the present constitutive-driver implementation of biaxial Willam's test, a first comparison is made to numerical results recently provided by Wosatko et al. (2020), who investigated, among other material models, the response of the CDP model at variable CDP dilatancy angle $\psi'_d = \tan^{-1} \alpha'_d$, under Willam's test, mainly by neglecting damage effects (plasticity-dominated responses). Indeed, thereby, the concrete material response also incorporating the effects of tensile damage function $D_t(\varepsilon_I^i)$ was delivered just for a single value of dilatancy angle ($\psi'_d =$ 25°). Here, such a latter case, and a pure elastoplastic response, assuming a rather considerable value of dilatancy angle ($\psi'_d =$ 55°), actually leading to non-zero negative asymptotic residual stresses, has been considered, for initial reproduction and validation purposes, starting from material parameters and functions as presented in Wosatko et al. (2020).

In Figure 3, the resulting in-plane Cartesian stress components, $\sigma_{11}, \sigma_{22}, \sigma_{12}$, and the arising principal stresses, σ_I, σ_{II}, are depicted against the prescribed strain along the x_1-axis, ε_{11}, which is assumed to be the true reference kinematic variable driving the material test (Figure 1), in all subsequent plots. The obtained responses look in rather good agreement with those earlier reported in (Wosatko et al., 2020), for all planar stress components, despite the limited accuracy that may be achieved in the attempt to graphically reconstruct their reported plots (both for input data and relative response outcomes).

The variations of normal stresses σ_{11} and σ_I reach at most a tensile value truly equal to the assumed concrete uniaxial tensile strength, $f_{t0} =$ 3.0 MPa, at the end of the first phase of Willam's test endowed with longitudinal elongation and lateral Poisson's contraction. Then, normal stresses σ_{11} and σ_I soften down along the post-peak range, during the second phase of Willam's test, endowed with biaxial elongation and shearing, but more rapidly than for a pure uniaxial strain-softening tensile response (as given by the imputed tensile strength curve), as per an effect of the mixed stress-strain conditions arising along the biaxial straining test.

Only when damage is truly made active ($D_t \neq 0$), do all stress components asymptotically approach zero at the final stage of full material disruption (Figure 3a), as $D_t \rightarrow 1$, i.e., with no non-zero residual stresses (non-negative for the transverse normal component). In fact, the full depletion of material integrity linked to damage and resulting stiffness degradation releases any possible residual stresses associated with plasticity processes, as linked to high inherent dilatancy, with respect to the kinematic constraints imposed by the test. This, in turn, comes to annihilate any appearance of plastic strain-induced anisotropy related to cumulated plastic strains, so that in the end, material behavior becomes isotropic, toward the asymptotic range of rather large strains.

As a matter of fact, as remarked by Wosatko et al. (2020), in stating that the CDP model, (in the purely plastic component) may not be able to satisfy one of the typical requirements of "passing" Willam's test (reaching a progressive annihilation of all stress components associated with increasing material degradation and complete disruption by microcracking). In fact, for a rather high value of dilatancy angle of the CDP model and in the absence of activated damage (Figure 3b), residual stresses arise at the end of the second extension/shearing phase of Willam's test. This result reflects the presence of non-zero effective stresses linked to choked in-plane dilatant plastic expansion, inherent of the plastic part of the model, as ruled by the assumed dilatancy angle in Equation 5, by virtue of the limited lateral contraction imposed by the assumed kinematics of the test during its second inelastic phase. This dilatant plastic flow and relevant effects reflect the pure plastic nature of the modeled material behavior by the CDP model, once elastic degradation is not activated. Like that, minor principal stress σ_{II} becomes negative (compression), as σ_I decreases to keep an almost constant gap with σ_{II}, equal to twice shear stress σ_{12}, as determined by the residual friction angle linked to the modified DP-like yield function. This issue can adequately be corrected by the addition of a slight amount of stiffness degradation, as illustrated in the sequel, through the re-parametrization and proposed effective handling of the CDP model, to provide a satisfactory material response under Willam's test, "passing" the test in all cases.

Moreover, one may notice one aspect of detail, in the recorded material responses: a closer look at Figure 3b around peak $\varepsilon_{11} = \varepsilon_{t0}$, $\varepsilon_{t0} = f_{t0}/E_0 \cong 0.0001$ being the elastic strain at the maximum reachable tensile stress, shows that both stresses σ_{22} and σ_{II} become negative, at the very beginning of the second phase of Willam's test, just before starting to grow towards positive values, as imposed vertical strain ε_{22} increases, also because of inherent plastic dilatancy. This local feature of the material response by the CDP model was presumably not made apparent in (Wosatko et al., 2020) and has been observed in this study only by setting a rather fine integration step, within the employed constitutive driver.

These first validation results, while corroborating the validity of the existing implementation, in adhering to outcomes from the

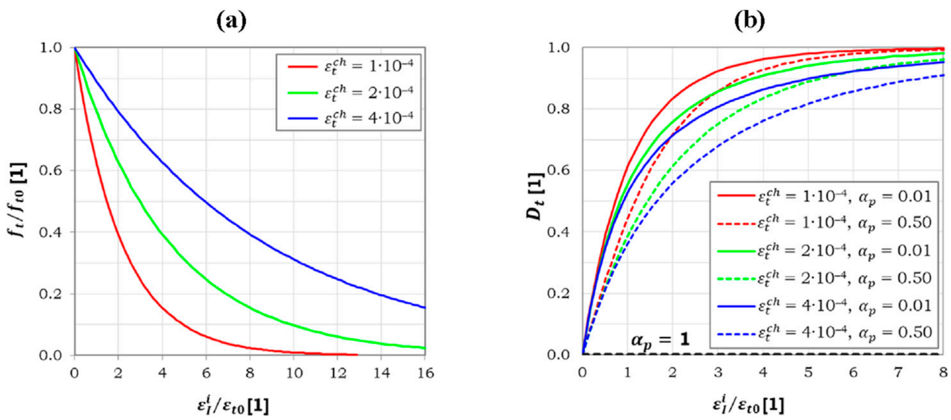

FIGURE 4
Prescribed parametrized functional evolution of concrete **(a)** tensile strength and **(b)** tensile damage as a function of major principal inelastic strain, for the considered values of characteristic constitutive parameters ε_t^{ch} and α_p.

existing literature on Willam's test, hint at a subsequent phase of development, for the re-parametrization and adequate tuning, of the CDP model, as it may be achieved by an external implementation. Thus, in order to provide, in any case, a correct interpretation of the material response under Willam's test, as it may be achieved by the available inherent characteristics, it is important to acknowledge its intrinsic limitations (such as the structural single-dissipative description, led by plastic deformation processes and the absence of damage-induced anisotropy, within the stiffness degradation processes), so that the CDP material model may be employed at its best, in the present potentialities, toward effective local and then global structural descriptions.

Thus, the next investigation forms both a way to adequately configure, or tune, the CDP material description and to set a comprehensive parametric analysis, to fully inspect the capabilities of the CDP model in "passing" and describing challenging benchmark biaxial Willam's test.

3.2 Extensive tuning and parametrization analysis

According to the above premises, to verify and extend the stated prodromal validation and emerging considerations and to accurately investigate the effect of inherent plastic dilatancy, brittleness, and damage description on the CDP model material response during biaxial extension/shearing Willam's test, a complete parametric investigation is set out at this stage, and extensively carried out; input and results are comprehensively discussed in Sections 3.2.1 and 3.2.2.

The numerical investigation is specifically focused on the following:

- The possibility to externally regularize or tune the constitutive description, in order to balance the effects of plastic strains and (isotropic) damage so that Willam's test can be "passed", with an arising consistent description, with features and potentialities to be investigated, first at a local constitutive scale, and next to a structural constitutive scale (subsequent Section 4).
- The purpose of providing an effective external parametrization of the CDP model, as it may be developed and separately be implemented, outside the running available FEM platform, by an informed expert user, to enhance the capabilities of the model description up to the maximum level of potentiality, within the intrinsic assumptions and limitations, to be completely understood, of the model.
- The interest in foreseeing the amount of strain-induced anisotropy, as driven by plastic strains and governed also by inherent (isotropic) damage, with progressive material annihilation due to diffused (and localized) microcracking, within the softening range.
- The capturing of the specific aspect of description of the rotations of the principal directions of stress beyond first cracking at the end of the first elongation phase of Willam's test, along the second extension/shearing phase, as it may be confronted with the outcomes of alternative, more sophisticated models (e.g., by anisotropic damage models).
- The enhancement of the CDP model, as scheduled in biaxial Willam's test, which may extend its capabilities over other loading scenarios, specifically at the structural scale, even in 3D, once the model is adopted in structural simulations, to describe concrete-like materials and resulting structural responses.

Toward these purposes, a complete external configuration and parametrization strategy of the CDP constitutive model is first originally attempted and described in the present contribution.

3.2.1 External parametrization of the constitutive law

The constitutive CDP model described in Section 2.1 allows the formulation of a variety of material behaviors by suitably varying the uniaxial post-peak strength and damage functions to be specified at the input stage in the inelastic range $(f_t(\varepsilon_t^i), f_c(\varepsilon_t^i), D_t(\varepsilon_c^i), D_c(\varepsilon_c^i))$

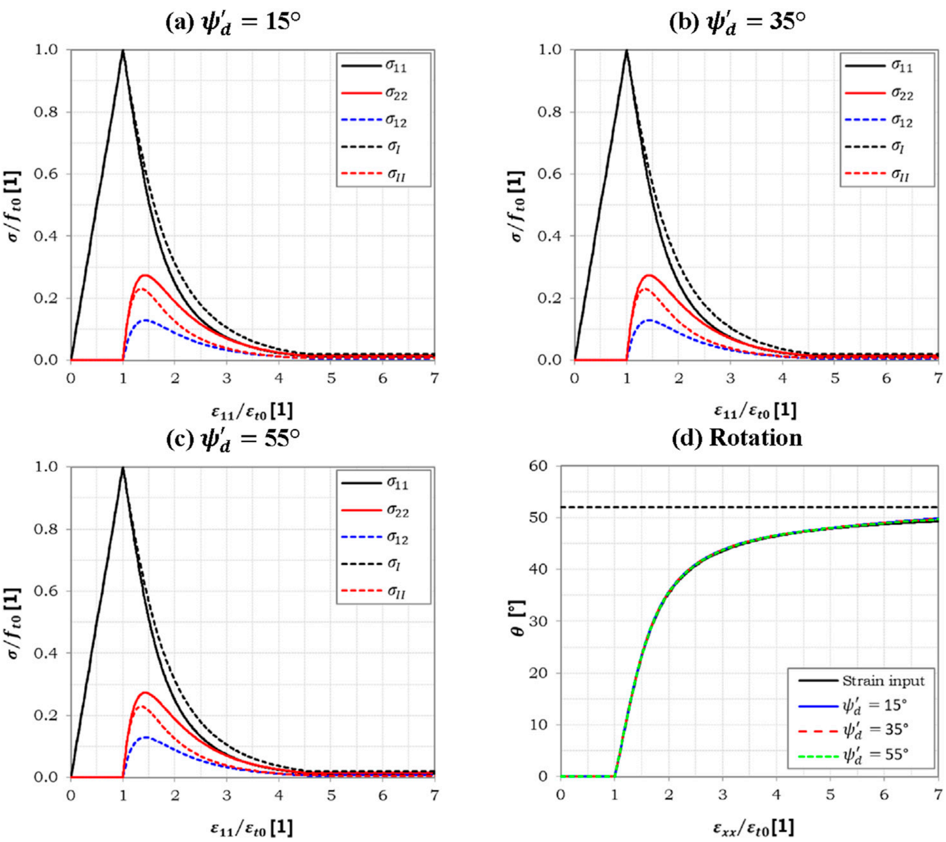

FIGURE 5
Response of CDP model under Willam's test: stress components calculated for dilatancy angles **(a)** $\psi'_d = 15°$, **(b)** $\psi'_d = 35°$ and **(c)** $\psi'_d = 55°$; **(d)** imposed rotation of the major principal strain axis and resulting rotation of the major principal stress axis. For $\varepsilon_t^{ch} = 1{\cdot}10^{-4}$ and $\alpha_p = 0.01$.

and the underlying constant characteristic material parameters to be set $(E_0, \nu_0, \alpha, \gamma, \psi'_d)$.

For extension and extension-shearing dominated problems, like Willam's test, the concrete nonlinear features of the material response in compression are basically un-mobilized. Thus, to minimize the present level of complexity, an adequate parametrization form of the CDP model, in tuning the amount of elastoplastic coupling, focused on the tensile description, may be achieved by appropriately defining functions $f_t(\varepsilon_t^i)$ and $D_t(\varepsilon_t^i)$ governing the concrete inelastic response under tensile-dominated stress-strain states, as driven by total inelastic tensile strain ($\varepsilon_t^i = \varepsilon_I^i$). Other parametrizations in terms of either plastic tensile strain ε_t^i or internal variable κ_t may also be feasible.

In the present analysis, a classical exponential decaying functional form of softening, e.g., (Bažant and Planas, 1998), is adopted, to externally describe the evolution of $f_t(\varepsilon_t^i)$, namely:

$$f_t(\varepsilon_t^i) = f_{t0}\exp\left(-\frac{f_{t0}}{g_t^f}\varepsilon_t^i\right) = f_{t0}\exp\left(-\frac{\varepsilon_t^i}{\varepsilon_t^{ch}}\right); \tag{18}$$

showing that exponential softening is completely specified by tensile strength f_{t0} of the undamaged concrete material and specific fracture energy in tension g_t^f. This may be condensed into a single softening material parameter governing such an exponential softening law, later considered in the parametric analysis, which is the characteristic tensile strain (Bažant and Planas, 1998) defined as:

$$\varepsilon_t^{ch} = \frac{g_t^f}{f_{t0}} = \frac{G_t^f}{f_{t0}h^e} = \varepsilon_{t0}\frac{E_0 G_t^f}{f_{t0}^2 h^e} = \frac{\varepsilon_{t0}}{\beta_H}; \tag{19}$$

where

$$\beta_H = \frac{h^e f_{t0}^2}{E_0 G_t^f}; \tag{20}$$

is the Hillerborg brittleness number (Bažant and Planas, 1998) that may be referred to finite element size h^e, as the reference structural dimension. Thus, the characteristic strain is a quantity infinitely large for the perfect plasticity limit ($\varepsilon_t^{ch} \to \infty$, $\beta_H \to 0$), i.e., when the Fracture Process Zone (FPZ) is much larger than the finite element size, and vanishingly small for the elastic-brittle limit ($\varepsilon_t^{ch} \to 0$, $\beta_H \to \infty$), i.e., when the FPZ is much smaller than h^e.

Clearly, one may see that the integration of Equation 18 over inelastic strain ε_I^i, from 0 to infinity, turns out exactly equal to g_t^f, which provides its meaning of specific fracture energy in tension. The fact that g_t^f is one of the inherent material parameters to be set may also be a convenient result for possibly implementing fracture-energy-based regularization procedures of strain localization at the finite element level and structural scale.

As defined above, in the CDP model the total inelastic strains are the sum of irrecoverable plastic strains due to plastic dissipation and

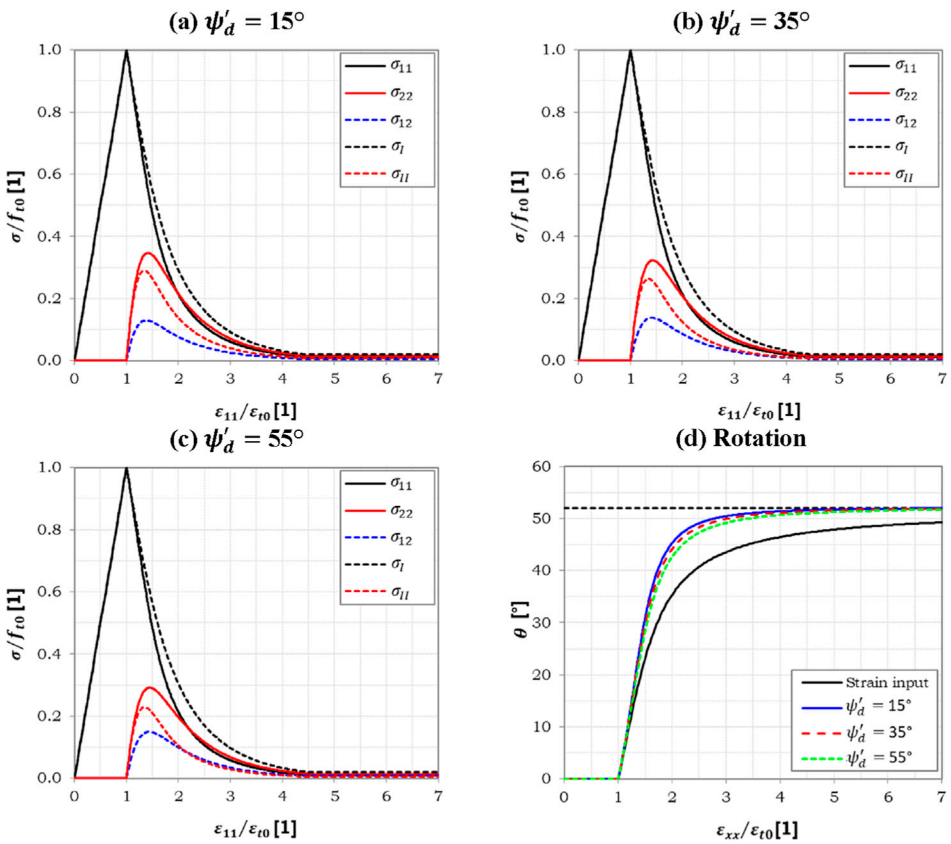

FIGURE 6
Response of CDP model under Willam's test: stress components calculated for dilatancy angles **(a)** $\psi'_d = 15°$, **(b)** $\psi'_d = 35°$ and **(c)** $\psi'_d = 55°$; **(d)** imposed rotation of the major principal strain axis and resulting rotation of the major principal stress axis. For $\varepsilon_t^{ch} = 1{\cdot}10^{-4}$ and $\alpha_p = 0.5$.

elastic-damage strains due to stiffness degradation, Equation 10. In ruling the balance of the two inelastic components, and phenomena, a convenient model to describe plasticity-driven microcracking may be obtained by further assuming that the plastic strain under tensile-dominated processes, is taken as a constant fraction of the total inelastic strain, say

$$\varepsilon_t^p = \alpha_p \varepsilon_t^i; \tag{21}$$

where $0 < \alpha_p \leq 1$ is a "plastic to inelastic strain ratio" parameter, in the spirit of Ortiz (1985), hereby considered as an external material constant, in ruling the functions to be set at input stage, for the CDP model. This allows for weighting the relative balance among plastic and damage processes, in the arising CDP material model response.

According to such a hypothesis, uniaxial tensile damage evolution function $D_t(\varepsilon_t^i)$, to be assigned in input for the CDP model, follows from above plastic to inelastic strain ratio α_p and from the assumed expression of $f_t(\varepsilon_t^i)$ given in Equation 18:

$$\varepsilon_t^i = \varepsilon_t^p + \varepsilon_t^{ed} = \alpha_p \varepsilon_t^i + \frac{D_t(\varepsilon_t^i)}{1 - D_t(\varepsilon_t^i)} \frac{f_t(\varepsilon_t^i)}{E_0}; \tag{22}$$

leading to

$$D_t(\varepsilon_t^i) = \left[1 + \frac{f_t(\varepsilon_t^i)}{(1 - \alpha_p) E_0 \varepsilon_t^i}\right]^{-1}. \tag{23}$$

The proposed external parametrization, allowing a tuning of the amount of elastoplastic coupling within the CDP model, may externally be set from the available computational platform (e.g., by a spreadsheet or any type of calculation script), without the need of a direct modification of the material description, e.g., by a user subroutine, through the adoption of a numerical or mathematical environment, or even a supporting spreadsheet, according to the main pseudo-coding steps resumed in the following flowchart (Table 1).

Both salient governing input tensile functions, $f_t(\varepsilon_t^i)$ in Equation 18 and $D_t(\varepsilon_I^i)$ in Equation 23, from the process above, are depicted in Figure 4, considering an undamaged Young's modulus of $E_0 = 21{,}500\ f_{t0}$, as for instance indicated by the CEB-FIP Model Code (1990) formula (Mehta and Monteiro, 2006), for a typical ratio of compressive/tensile strengths (f_{c0}/f_{t0}) equal to 10. In the present study, any stress response has been scaled to f_{t0}; thus, the value assigned to f_{t0} turns out to be irrelevant. The initial compressive strength $f_{c0} = 10 f_{t0}$ is hereby kept fixed during the analysis, focused on tensile-dominated response, due to its expected negligible effect during biaxial extension/shearing Willam's test. Poisson's ratio ν_0 of the virgin isotropic material is taken equal to 0.2.

Resulting tensile damage evolution function $D_t(\varepsilon_t^i)$ is plotted in Figure 4b for two separate values of plastic to inelastic strain ratio α_p. One value is rather small ($\alpha_p = 0.01$) but, still, greater than zero (inelasticity of the CDP model is truly driven by plastic

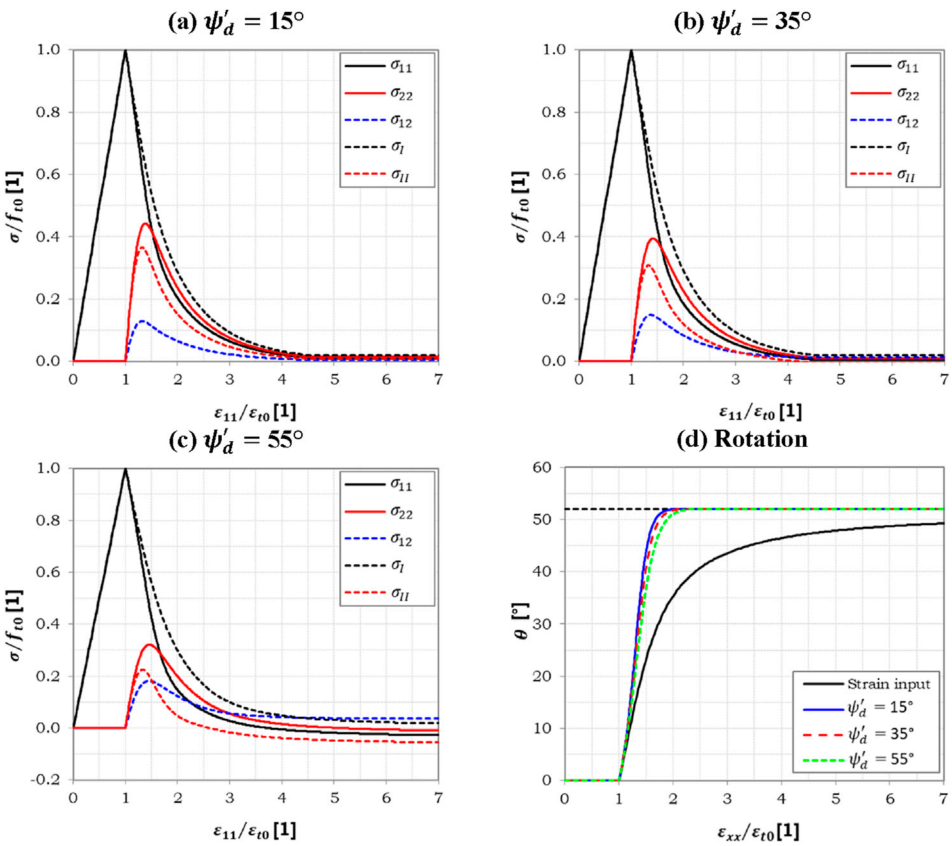

FIGURE 7
Response of CDP model under Willam's test: stress components calculated for dilatancy angles **(a)** $\psi'_d = 15°$, **(b)** $\psi'_d = 35°$ and **(c)** $\psi'_d = 55°$; **(d)** imposed rotation of the major principal strain axis and resulting rotation of the major principal stress axis. For $\varepsilon_t^{ch} = 1{\cdot}10^{-4}$ and $\alpha_p = 1.0$.

strains, which cannot be suppressed), indicating a dominant damage model with nearly isotropic damage and negligible plasticity. The other value is placed right in the middle of the admissible α_p range ($\alpha_p = 0.5$), leading to a plastic-damage model with mid elastoplastic coupling, in which both plastic flow and stiffness degradation equally contribute to the total inelastic strains ($\alpha_p = 0.5$). Notice that upper limit $\alpha_p = 1$, referring to a CDP model degenerating into a pure softening elastoplastic formulation (with no inherent damage), is considered in the present analysis, even though it may lead to "failing" Willam's test, as earlier discussed in (Wosatko et al., 2020), about the requirement of no residual stresses on the asymptotic tail of the softening range.

The remaining characteristic material parameters of the CDP model are kept fixed to their common values as follows: eccentricity of the plastic potential $e = 0.1$; shape parameters of the yield function, namely $\alpha = 0.121$, corresponding to a ratio of biaxial to uniaxial compressive strengths of 1.16, and $\gamma = 3$, obtained by setting the ratio between the radii of tensile and compressive meridians on the deviatoric plane to the standard value of 2/3.

3.2.2 Parametrized responses to Willam's test

The previous constitutive parametrized description (Equations 18–23) relies on three main material parameters, in the present analysis taken as variable ones, with all other material constants fixed as said, to explore the capabilities of the so-tuned CDP constitutive model under biaxial Willam's test: characteristic tensile softening strain $\varepsilon_t^{ch} = g_t^f / f_{t0}$, plastic to inelastic strain ratio $\alpha_p = \varepsilon_t^p / \varepsilon_t^i$ and inherent CDP dilatancy angle $\psi'_d = \tan^{-1} \alpha'_d$ (directly fixed within the originally coded formulation).

An extensive parametrization analysis is then made, and in the investigation specifically reported for the following:

- ε_t^{ch} equal to the three characteristic values of $1 \cdot 10^{-4}$, $2 \cdot 10^{-4}$, $4 \cdot 10^{-4}$ (setting an increasing value of specific tensile fracture energy g_t^f at fixed peak stress f_{t0}, i.e., an increasing ductility of enduring tensile softening tail at increasing strains);
- α_p equal to the three characteristic values of 0.01, 0.50, 1.00 (ranging from negligible plasticity or almost pure damage, to mid plasticity/damage, to pure plasticity or no damage);
- ψ'_d equal to the three characteristic vales of 15°, 35°, 55° (CDP dilatancy angles encompassing a range of possibly expected experimental values for concrete, ranging from moderate to high dilatancy).

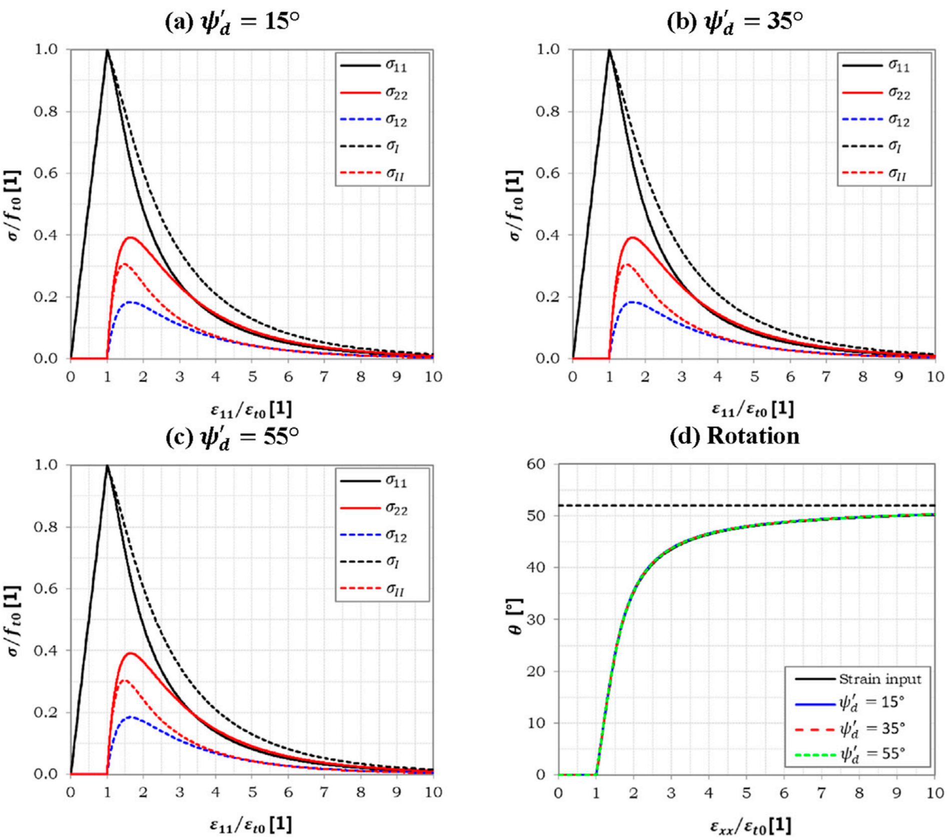

FIGURE 8
Response of CDP model under Willam's test: stress components calculated for dilatancy angles **(a)** $\psi'_d = 15°$, **(b)** $\psi'_d = 35°$ and **(c)** $\psi'_d = 55°$; **(d)** imposed rotation of the major principal strain axis and resulting rotation of the major principal stress axis. For $\varepsilon_t^{ch} = 2{\cdot}10^{-4}$ and $\alpha_p = 0.01$.

Graphical representations of the normalized constitutive response of the CDP model for all in-plane stress components, both Cartesian and principal, acquired from the constitutive driver, single finite element, numerical simulation of biaxial Willam's test are extensively provided in Figures 5–13; in each, for the three assumed values of CDP dilatancy angle ψ'_d, (a) to (c); while, in the same, frames (d) report the input/obtained rotation of major principal strain/stress directions. Figures 5–13 wholly illustrate the outcomes of the extensive parametric analysis that has been conducted in the present study and delivered in the evidence reported in the paper. Specific and general considerations and differences, among the various recorded material responses, are exposed in detail in what follows.

For $\alpha_p = 0.01$ (negligible plasticity though still driving single-dissipative inelasticity with prevailing damage), the resulting stress response looks consistently unaffected by the inherent dilatancy angle (Figures 5a–c, 8a–c, 11a–c) since plastic strains take a minimum weight in the total inelastic strains and are as such kept to a minimum, while the overall inelastic process is mainly attributed to (isotropic) stiffness degradation linked to tensile damage. Accordingly, as expected from the underlying isotropy considerations and above statements, the resulting principal stress directions practically coincide with the prescribed principal strain directions, i.e., principal stress-strain axes co-rotate, with each other, independently of CDP dilatancy angle ψ'_d (Figures 5d, 8d, 11d). Only at rather large driving external strains (say, e.g., $\varepsilon_{11} > 6\varepsilon_{t0} = 6 f_{t0}/E_0$) may some slight deviations from coaxiality be appreciated, due to the development, in the end, of small plastic strains. Hence, the achieved numerical outcomes corroborate the theoretical statements of preceding Section 2.3, in that no material anisotropy is actually manifested by the constitutive model, even in the peculiar biaxial extension/shearing contest of Willam's test, whenever plastic strains remain marginal (though still driving the whole inelastic process).

For $\alpha_p = 0.50$ (mid elastoplastic coupling), non-negligible plastic strains are accounted for, during the second phase of biaxial Willam's test, and in the stress responses (Figures 6a–c, 9a–c, 12a–c); both σ_{22} and σ_{12} stress components increase with respect to those predicted by a "pure" damage model ($\alpha_p = 0.01$), because of the damped stiffness degradation, attested by what was set in input in Figure 4b. Also, the increase of σ_{22} is such that, at some point, it overcomes σ_{11} independently from ψ'_d, a feature also revealed by other more sophisticated constitutive models tried along with biaxial Willam's test [e.g. (Carol et al., 2001b; Meschke et al., 1998)]. As concrete dilatancy rises, for fixed total strains, plastic strain growth occurs, to the detriment of elastic strains, thus reducing σ_{22} and σ_{II}; on the other hand, shear stress component σ_{12} somewhat benefits from such an additional compressive strength promoted by dilatancy, while its dependence on α_p seems marginal.

For $\alpha_p = 1.00$ (no damage, pure plastic behavior), one first appreciates in Figures 7a–c, 10a–c, 13a–c the possibility of residual

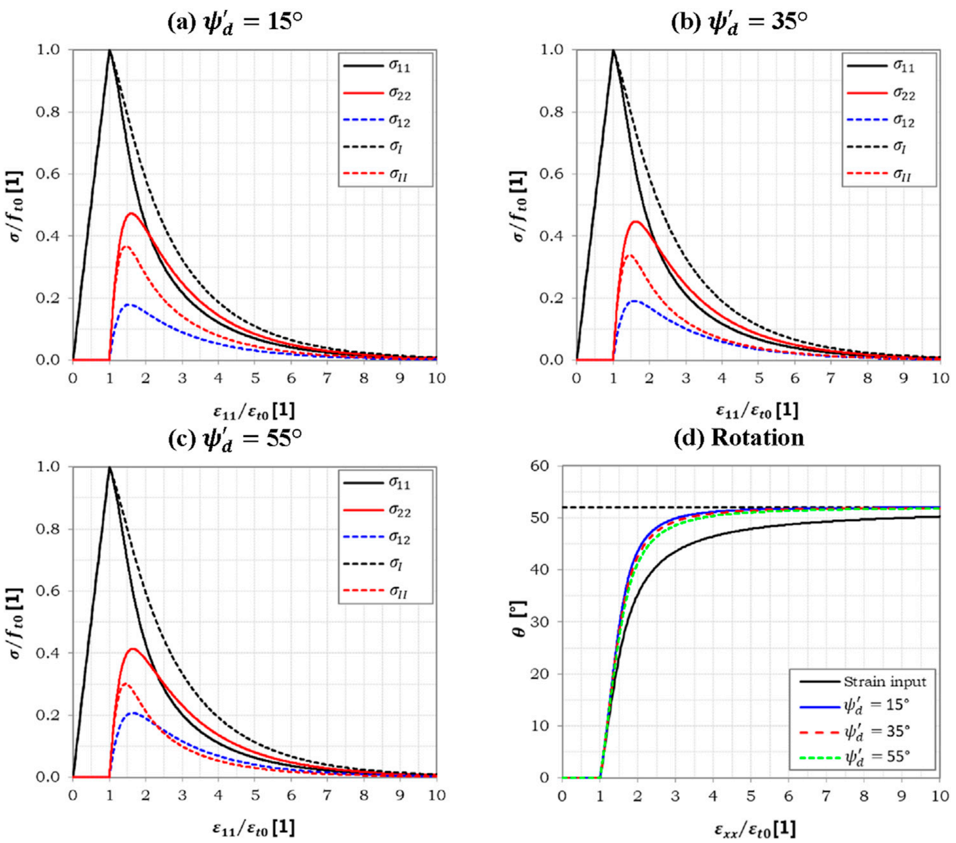

FIGURE 9
Response of CDP model under Willam's test: stress components calculated for dilatancy angles **(a)** $\psi'_d = 15°$, **(b)** $\psi'_d = 35°$ and **(c)** $\psi'_d = 55°$; **(d)** imposed rotation of the major principal strain axis and resulting rotation of the major principal stress axis. For $\varepsilon_t^{ch} = 2{\cdot}10^{-4}$ and $\alpha_p = 0.50$.

asymptotic stresses to appear in the softening tail, as per formally a failure in "passing" Willam's test [as stated in (Wosatko et al., 2020)], which the devised tuning strategy may anyway readily regularize, by setting an appropriate strain ratio parameter below one, $\alpha_p < 1$, reaching an effective tuning of the CDP model, and allowing for its potential applications in real concrete material and structural computational contexts.

The plots of the angle of rotation of principal stress directions (Figures 7d, 10d, 13d) substantially differ from that of the "pure" isotropic damage case (Figures 5d, 8d, 11d), revealing that plastic strain-induced anisotropy does accelerate the rotation of principal stresses, almost independently of the value of the inherent CDP dilatancy angle. The positive values of plastic strains (opening microcracks), as described by the normal to the DP-like plastic potential in the plastic flow rule, shall explain why stress increments over-rotate with respect to strain increments. All rotation trends turn out to be upper bounded by asymptotic strain angle 52.02°, since they never exceed that value, at this simulation material level, as instead possibly obtained by different, more sophisticated anisotropic damage models [e.g. (Carol et al., 2001a; Carol et al., 2001b; Oliver et al., 1990)]. However, at the constitutive structural scale, once imperfection-triggered strain localization occurs, during Willam's test, resulting macroscopic responses become richer, and surprisingly near the above features of anisotropic damage models, by a much higher effect of inelastic-induced anisotropy. This is further discussed in Section 4.

Also, from Figures 7d, 10d, 13d, it is apparent that the rotation rate of the principal stress components is drastically reduced, say at around $\varepsilon_{11} = 3\varepsilon_{t0}$, and gradually converges towards the final asymptotic value of imposed strain rotation. In fact, as an important remark, out of the present analysis, as the prescribed driving strains increase, inherent damage progressively withdraws plastic strain-induced-anisotropy, so that material behavior tends to return fully isotropic, in the limit of very large strains, as predicted by the CDP model, when some damage participation in the elastoplastic coupling is turned on ($\alpha_p < 1$). This statement is confirmed by the rotation of principal strain frame obtained for the mid elastoplastic coupling condition ($\alpha_p = 0.5$), as depicted in Figures 6d, 9d, 12d.

As per the effect of ε_t^{ch} (or β_H), namely of the amount of enduring "ductility" in the imputed exponential softening tail, at increasing specific fracture energy g_t^f, one clearly appreciates the enlarged extensions of the resulting softening branches, represented in Figures 8–13 with different strain ranges. Also, levels of secondary stress components (i.e., non σ_{11} stress) become much higher, at increasing g_t^f, showing much more resilient behavior. On the other hand, maximum over-rotation $\Delta\theta_M$ of principal stress directions with respect to the principal strain frame decreases

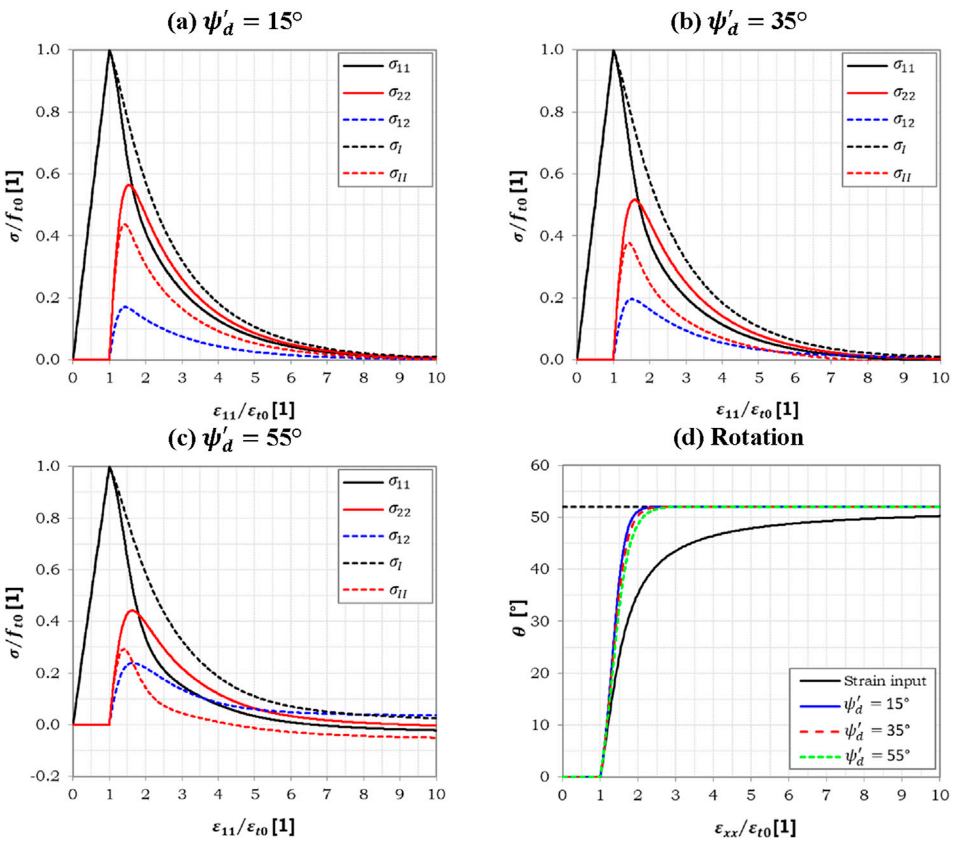

FIGURE 10
Response of CDP model under Willam's test: stress components calculated for dilatancy angles **(a)** $\psi'_d = 15°$, **(b)** $\psi'_d = 35°$ and **(c)** $\psi'_d = 55°$; **(d)** imposed rotation of the major principal strain axis and resulting rotation of the major principal stress axis. For $\varepsilon_t^{ch} = 2{\cdot}10^{-4}$ and $\alpha_p = 1.00$.

as ε_t^{ch} increases (compare either Figure 6d with Figure 12d or Figure 7d with Figure 13d), for any value of ψ'_d and $\alpha_p < 1$, as the more quasi-brittle the material is, the more plastic strains develop at the beginning of the second phase of the test.

Finally, Figure 14 also depicts resuming frames for the dispersion of main resulting material features, such as peak stresses and maximum stress-to-strain over-rotation at variable parameters ε_t^{ch} and α_p, for the three taken values of dilatancy angles ψ'_d, confirming the previously stated observations. This shows that the stated external tuning strategy and parameters allow to represent a good range of material responses, to be tailored to the specific material behavior at hand. Distribution seems a little wider, which looks good, toward model versatility, for moderate dilatancy angles, which may be more typical for real concrete behaviors.

4 Structural constitutive simulations of biaxial Willam's test

In view of investigating the performance of the CDP model at the constitutive structural scale of a specimen size, further numerical simulations of biaxial extension/shearing Willam's test are now formed, with different regular FEM discretizations, in order to inspect how the local and global response is affected, specifically with respect to homogeneity, potential inelastic-induced anisotropy, resulting macroscopic bearing capacity, and possible onset of strain localization.

In the present study, the issue of regularization, of the computational formulation, and objectivity of the overall structural response, in the possible presence of strain localization, is tackled by a standard fracture-energy-based regularization ($g_t^f = G_t^f/h^e$) of the local CDP model, as available within the FEM code at hand (ABAQUS).

Toward that, according to the following two subsections, two separate campaigns of numerical simulations are developed:

- First is a campaign with no triggering imperfections, meant to inspect if homogeneity is preserved, at the specimen structural scale, as per the preceding single-element campaign.
- Second is a campaign with a triggering (geometrical) imperfection (slight deviation of a node coordinate), as conceived to explore a possible onset of strain localization and to observe macroscopic features of specimen response, with arising inelastic-induced anisotropy within the discretized structural element.

Therein, two different regular FEM discretizations of a square specimen by square linear quadrilateral finite elements

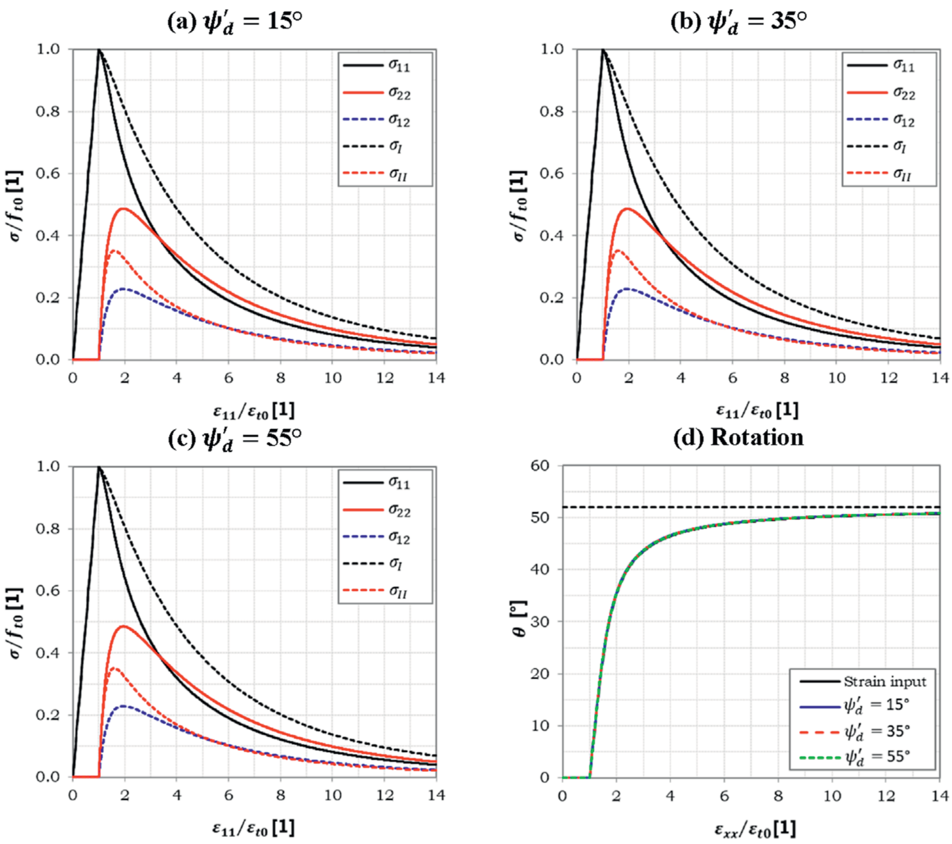

FIGURE 11
Response of CDP model under Willam's test: stress components calculated for dilatancy angles **(a)** $\psi'_d = 15°$, **(b)** $\psi'_d = 35°$ and **(c)** $\psi'_d = 55°$; **(d)** imposed rotation of the major principal strain axis and resulting rotation of the major principal stress axis. For $\varepsilon_t^{ch} = 4{\cdot}10^{-4}$ and $\alpha_p = 0.01$.

(8 × 8, 32 × 32) with reduced integration are considered, as shown in Figure 15. Kinematic constraints of Willam's test are imposed, at the external boundaries, through an autonomously implemented ABAQUS User-Subroutine (ABAQUS, 2025), written in the Fortran programming language, to reproduce the meant kinematic displacement-controlled deformation field depicted in Figure 2b.

Since the boundary conditions of Willam's test belong to the class of so-called Kinematic Uniform Boundary Conditions (KUBC) (Besson et al., 2010), the overall response of the discretized specimen may be homogenized by taking the spatial average of both stress and strain tensor fields over the specimen. In fact, under KUBC, Hill's macro-homogeneity condition,

$$\left\langle \sigma_{ij}\dot{\varepsilon}_{ij} \right\rangle_V = \left\langle \sigma_{ij} \right\rangle_V \left\langle \dot{\varepsilon}_{ij} \right\rangle_V, \tag{24}$$

holds [Hill-Mandel lemma (Besson et al., 2010)], where $\langle \cdot \rangle_V$ denotes the spatial average operator over volume V. Equation 24 states that the virtual work associated with the homogenized (macroscopic) stresses and strains must equal the volume-averaged work associated with the punctual (microscopic) stresses and strains. This, in turn, means that the homogenized structural response of the specimen is thermodynamically equivalent to its complete field response, as numerically evaluated by the finite element analysis. Moreover, the form of the equilibrium equations does not change when transitioning from the single finite element (microscale) to the overall structure (macroscale) (Besson et al., 2010).

The results of the numerical experiments, performed at fixed $\varepsilon_t^{ch} = 1 \cdot 10^{-4}$ and $\alpha_p = 0.50$, for the three values of ψ'_d already considered at the constitutive-driver scale, are presented in the forthcoming subsections.

4.1 Homogeneous response at variable discretization

Once the model outline has no imposed imperfections, the global response is indeed homogeneous, within the specimen, and is basically reproducing the pure constitutive response (of a single finite element), as already presented and discussed in the previous sections. This is demonstrated in Figure 16, where the resulting homogenized stress-strain responses are reported, displaying features similar to those earlier expressed by the constitutive modelization with a single finite element, at the pure local stress-strain scale.

Figure 17 further illustrates the deformed configuration of the specimen together with the corresponding displacement magnitude, $\|u_i\| = \sqrt{u_i u_i}$, the spatial distributions of scalar damage variable D, and of maximum principal plastic strain ε_I^p at the end of Willam's test ($\varepsilon_{11} = 8.5\varepsilon_{t0}$), for the two considered squared meshes, for the case $\psi'_d = 35°$. The perfect homogeneity of the numerically evaluated

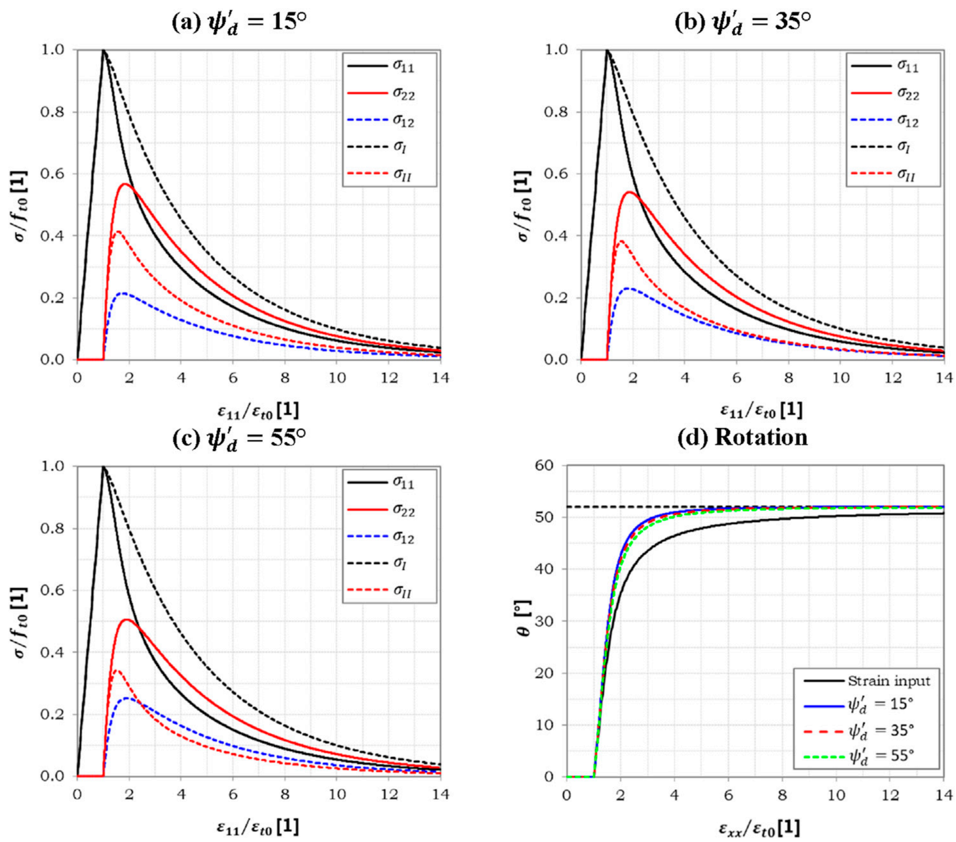

FIGURE 12
Response of CDP model under Willam's test: stress components calculated for dilatancy angles **(a)** $\psi'_d = 15°$, **(b)** $\psi'_d = 35°$ and **(c)** $\psi'_d = 55°$; **(d)** imposed rotation of the major principal strain axis and resulting rotation of the major principal stress axis. For $\varepsilon_t^{ch} = 4{\cdot}10^{-4}$ and $\alpha_p = 0.5$.

fields ensues from the spatially uniformity of the imposed strain field of Willam's test. In fact, the shape functions of the linear quadrilateral elements adopted in the analysis allow one to exactly reproduce the imposed constant strain field. Thus, the numerical solution is not influenced by either the number or the position of the Gauss points (no quadrature error in the stiffness matrix assembly), as in the known Patch test (Zienkiewicz et al., 2013). This provides further illustration and corroboration of the present capabilities of the so-tuned CDP model under biaxial Willam's test.

Thus, no appearance of strain localization is recorded, and features and capabilities of the CDP model, with present external parametrization enhancement, can effectively tune the amount of elastoplastic coupling, the result of which conforms to the expectations of Willam's test, also at high inherent plastic dilatancy, once some damage coupling is present, are revealed, in reproducing the outcomes of the CDP model, as seen at a pure constitutive-driver scale. Notice that, in this case, no fracture-energy-based regularization has explicitly been introduced, due to the absence of any strain localization phenomena.

Specifically, without appearance of strain localization, the amount of inelastic-induced anisotropy remains again rather confined, both during the initial softening phase in the second part of the test and along its tail, toward the end of it, where the response behavior basically returns isotropic, in the progressive annihilation of material bearing capacity as linked to even mild stiffness degradation, and even in case of pure plasticity, at rather large total (plastic-dominated) strains.

4.2 Triggered strain-localization response at variable discretization

Once potential strain localization is triggered by a (geometrical) imperfection (e.g., displaced node coordinate), results become very interesting, and actually surprisingly intriguing, for the capabilities of the CDP model at the structural scale, under biaxial Willam's test. The imposed geometrical imperfection consists of a perturbation of the x_2 coordinate of the central bottom node highlighted in Figure 15, equal to one thousandth of the square side. The previously mentioned standard fracture-energy-based regularization has been enforced now, to limit mesh-objectivity issues related to strain localization.

Strain localization indeed appears, initially at the end of the first phase of the test, and becomes noticeable in the second softening phase of the test (see evolutions of stress components in Figure 18 vs. in Figure 16), as it may be appreciated in Figure 19 ($\varepsilon_{11} = 8.5\varepsilon_{t0}$). The extension/shearing test leads to smeared and localized deformation patterns at the end of Willam's test, with an inclined macroscopic crack band across the specimen scale, as described by the CDP elastoplastic coupling description.

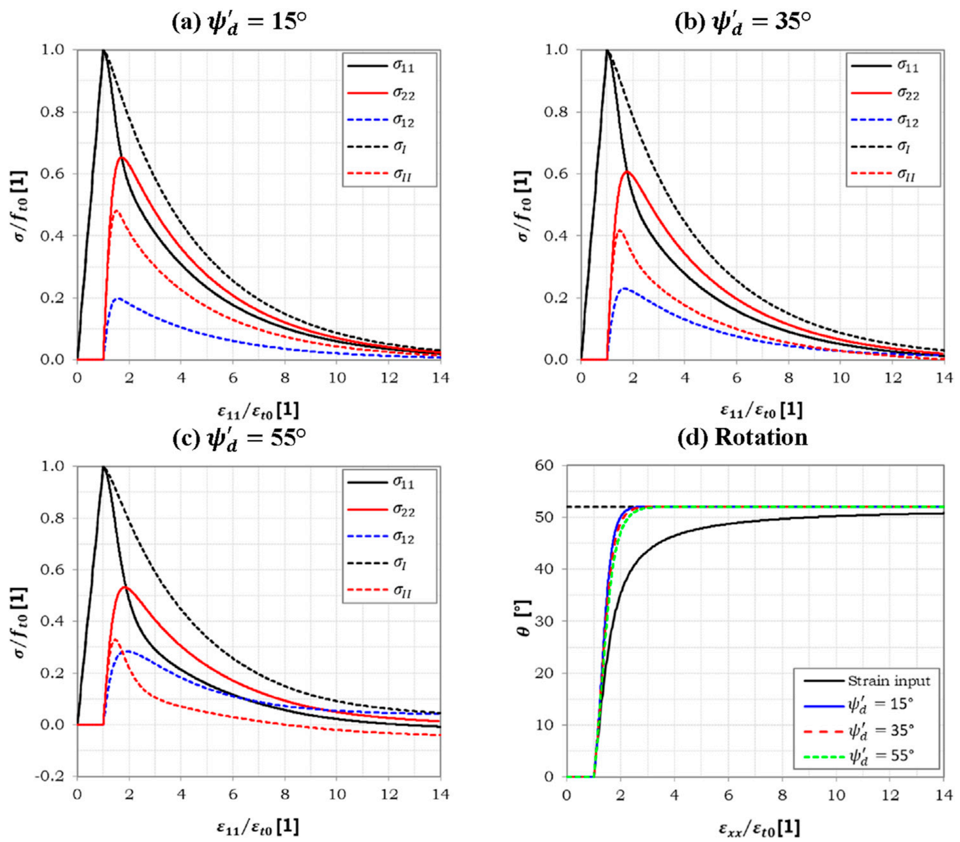

FIGURE 13
Response of CDP model under Willam's test: stress components calculated for dilatancy angles **(a)** $\psi'_d = 15°$, **(b)** $\psi'_d = 35°$ and **(c)** $\psi'_d = 55°$; **(d)** imposed rotation of the major principal strain axis and resulting rotation of the major principal stress axis. For $\varepsilon_t^{ch} = 4{\cdot}10^{-4}$ and $\alpha_p = 1.0$.

Features are rather rich in appearance also at changing constitutive variables and discretizations. The displacement field shows a clear localization pattern triggered by the introduced imperfection, depending on the finite element size. For the coarse mesh (8 × 8), the displacement band is broader and blunt, while displacements localize more distinctly along a narrow band for the finer mesh (32 × 32); thus, the improved spatial resolution better captures the localization behavior.

Damage evolution is strongly influenced by the adopted mesh. The coarse mesh displays a diffused damage zone, spreading over a wider region. The fine mesh shows a more concentrated damage band aligned with the expected localization direction, demonstrating higher fidelity in representing damage gradients. Plastic strain accumulation mirrors the damage patterns. The 8 × 8 mesh yields a smeared response, where maximum plastic strain affects several elements. The 32 × 32 mesh produces a narrow, sharply defined localization zone with higher peak strain, which is characteristic of strain-softening materials undergoing localized failure. Thus, the dominant cracking path, as given by the locus of the trajectories of the plasticized elements at the macroscopic level, is strongly affected by the finite element discretization.

Hence, the present outcomes confirm that the imperfection successfully triggers strain localization and that mesh refinement significantly enhances the accuracy of capturing displacement, damage, and plastic-strain localization. The contrast between the two meshes highlights the importance of spatial resolution when modeling strain-softening phenomena that involve loading conditions, such as those of biaxial Willam's test.

Moreover, global responses are extracted, from the aforementioned equivalent averaging process, resulting in further multifaceted features, specifically in terms of inelastic-induced anisotropy, at the structural scale, as shown in Figures 19, 20. The possibility to transmit compression and shear stresses along the localization band raises the mean value of all the stress components, especially σ_{22}, and produces a more extended post-peak softening branch, with the appearance of small residual stresses, i.e., a higher overall ductility of the specimen is retrieved.

Astonishingly, as a main iconic and condensing result of the present investigation, in terms of over-rotation among principal stress and strain directions (Figure 20), further richer manifestations are recorded, for the in essence isotropic CDP model, nearing characteristics that have been observed, at the pure material scale, by more sophisticated constitutive models, such as for instance for anisotropic damage models [e.g., (Carol et al., 2001a); (Carol et al., 2001b); (Carol et al., 2008)]. Thereby, stress over-rotations go over the targeted asymptotic strain rotation, of near 52°, as imposed by the controlled kinematics of Willam's test, while later relaxing down toward it, from above, along with complete material annihilation.

10.3389/fmats.2026.1800938

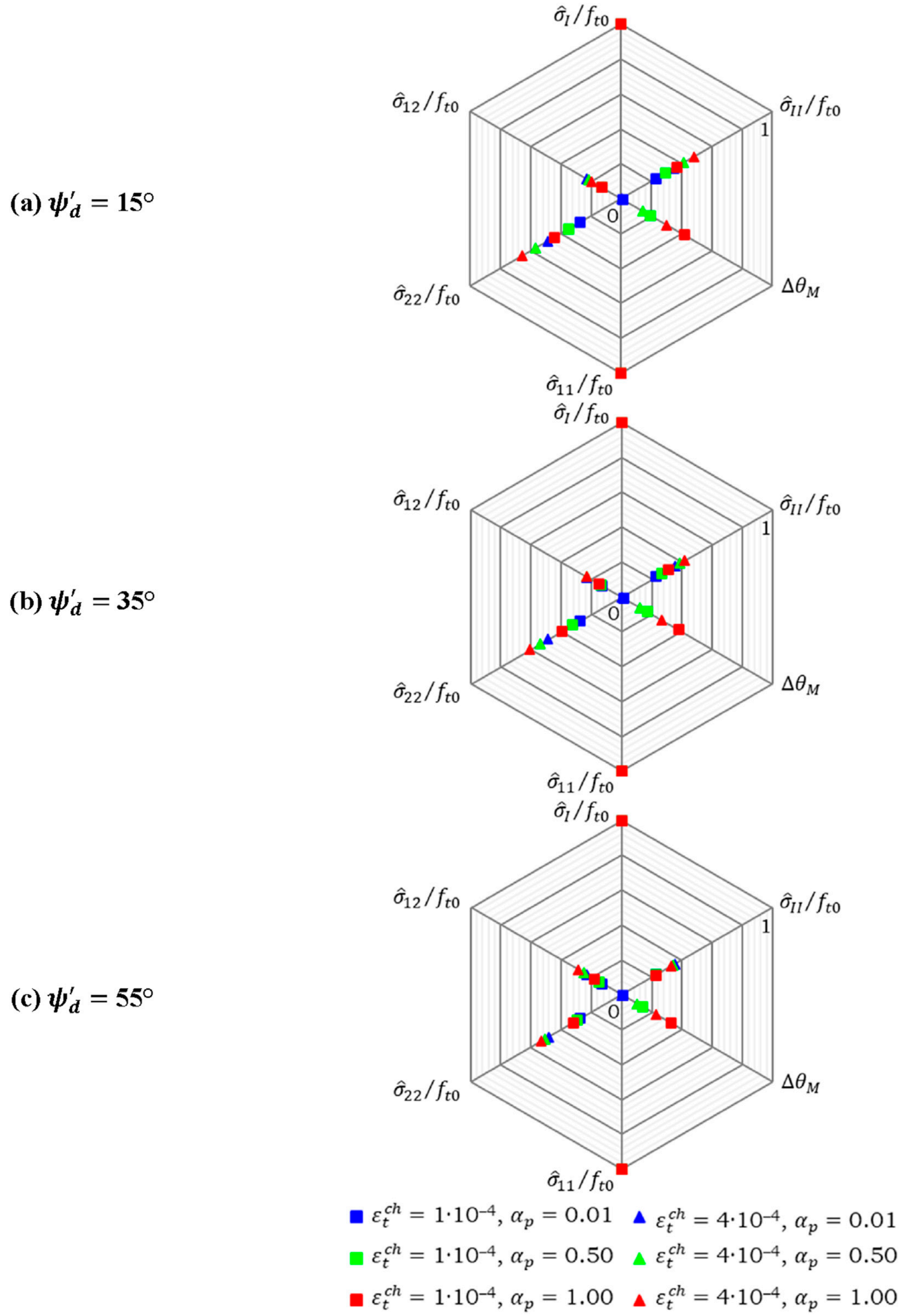

FIGURE 14
Variation of peak Cartesian stresses, peak principal stresses, and maximum normalized relative rotation of principal stress directions with respect to principal strain directions at variable ε_t^{ch} and α_p, for **(a)** $\psi'_d = 15°$, **(b)** $\psi'_d = 35°$, and **(c)** $\psi'_d = 55°$.

10.3389/fmats.2026.1800938

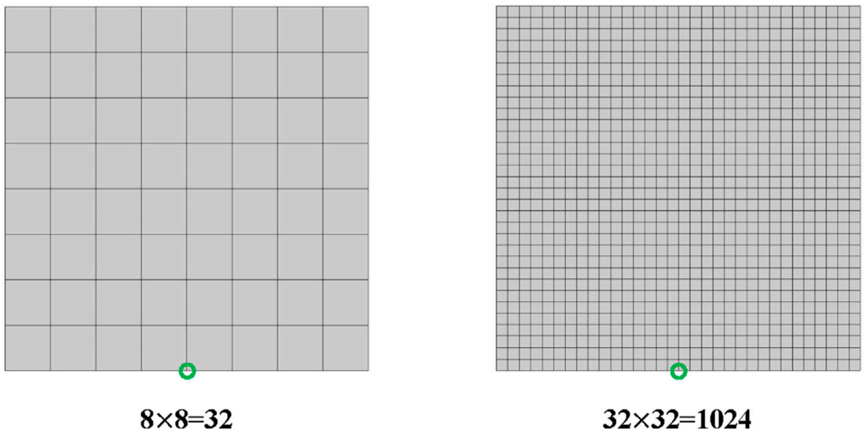

FIGURE 15
Adopted quadrilateral finite element discretizations of the quadrilateral specimen subjected to biaxial Willam's test. The green circle points to the node where a little geometrical imperfection is imposed to trigger strain localization.

As such, this is a specific and rather interesting observed feature of the CDP model capability that may display further implications in real structural scales, for instance in the simulations of large-scale concrete structures, as dealt at the continuum scale, by smeared constitutive models (stress-strain laws) with non-linear energy-dissipation capabilities.

This shows that, despite inherent simplicity, and main isotropic constitutional outline, the CDP model shall anyway show promise, in terms of practical applications, for first-level and achievable treatment of concrete structures by (local) smeared approaches, in allowing one to trace the non-linear range of response, with adequate description of the post-peak branches, in the assessment of residual load-carrying capacity and enduring ductility in terms of displacement-based performance, design, and safety assessment.

About "damage-induced softening" vs. "plastic softening", in terms of strain localization appearance, at the specimen structural scale of interest, such a process is anyway led, as per the underlying driving force, by plastic deformation processes. Despite this, the arising localization phenomenon is highly marked by the recorded concentration of damage patterns, as linked to the resulting stiffness degradation, within the localization zone, as visible in Figure 19. Thus, if one may say that the underlying driving variable of the inelastic processes, given the single-dissipative nature (Rizzi et al., 1996) of the CDP model, is anyway attributed to plastic phenomena, progressive and localized material bearing capacity annihilation is brought to light by the linked damage process, in terms of stiffness degradation associated to microcracking. Like that, the form of recorded strain localization is in between, and composed of, that of a pure elastoplastic process and that of a pure stiffness degradation or damage process, and that indeed lies in the intended "elastoplastic coupling" (Hueckel and Maier, 1977; Maier and Hueckel, 1979), as an underlying material framework of the inelastic CDP model. The analysis presented in the paper reveals peculiar features that may be achieved, at the mere material and structural specimen scales, by this type of coupled models. On this issue, additional analysis and inspection may be the subject of further work.

5 Conclusions

In the present research investigation, the rather popular Lee-Fenves' so-called Concrete Damaged Plasticity (CDP) constitutive model (available within the ABAQUS FEM platform), which still constitutes the subject of current research interest [e.g., (Wosatko et al., 2020)], has been reconsidered, analyzed, and parametrized, toward achieving effective tuning and flexibility, in order to inspect its current abilities and possible limitations in the material description of the nonlinear behavior of quasi-brittle materials, such as concrete, under complex loading paths, such as those involved in rather well-known and challenging benchmark biaxial extension/shearing Willam's test (Willam et al., 1987), originally conceived to assess the response of either fixed or rotating smeared-crack models.

Specifically, this study has been conceived with the intention of investigating the potentialities of representation of inelastic-induced anisotropy, at the material scale and at the specimen structural scale, under multiaxial stress-strain states, also with potential manifestations of strain localization, as described at the continuum scale by smeared material models, to move later on to the full structural scale, as e.g., that of large-scale concrete structures, in either static or dynamic scenarios, including for design and safety assessment under challenging loading conditions that may promote nonlinear responses and even lead to progressive damage and eventual failure.

The constitutive assessment analysis has been organized in three main parts, in which the following main issues have been addressed:

a) Analysis of inherent constitutive formulation and resulting recordable effect of inelastic-induced anisotropy, in general terms and in the specific case of biaxial extension/shearing Willam's test, once seen at the material level, by a constitutive-driver simulation scale within the use of a single finite element with a single integration point.
b) External parametrization description and tuning of the CDP model, specifically for the need of balancing the amount

10.3389/fmats.2026.1800938

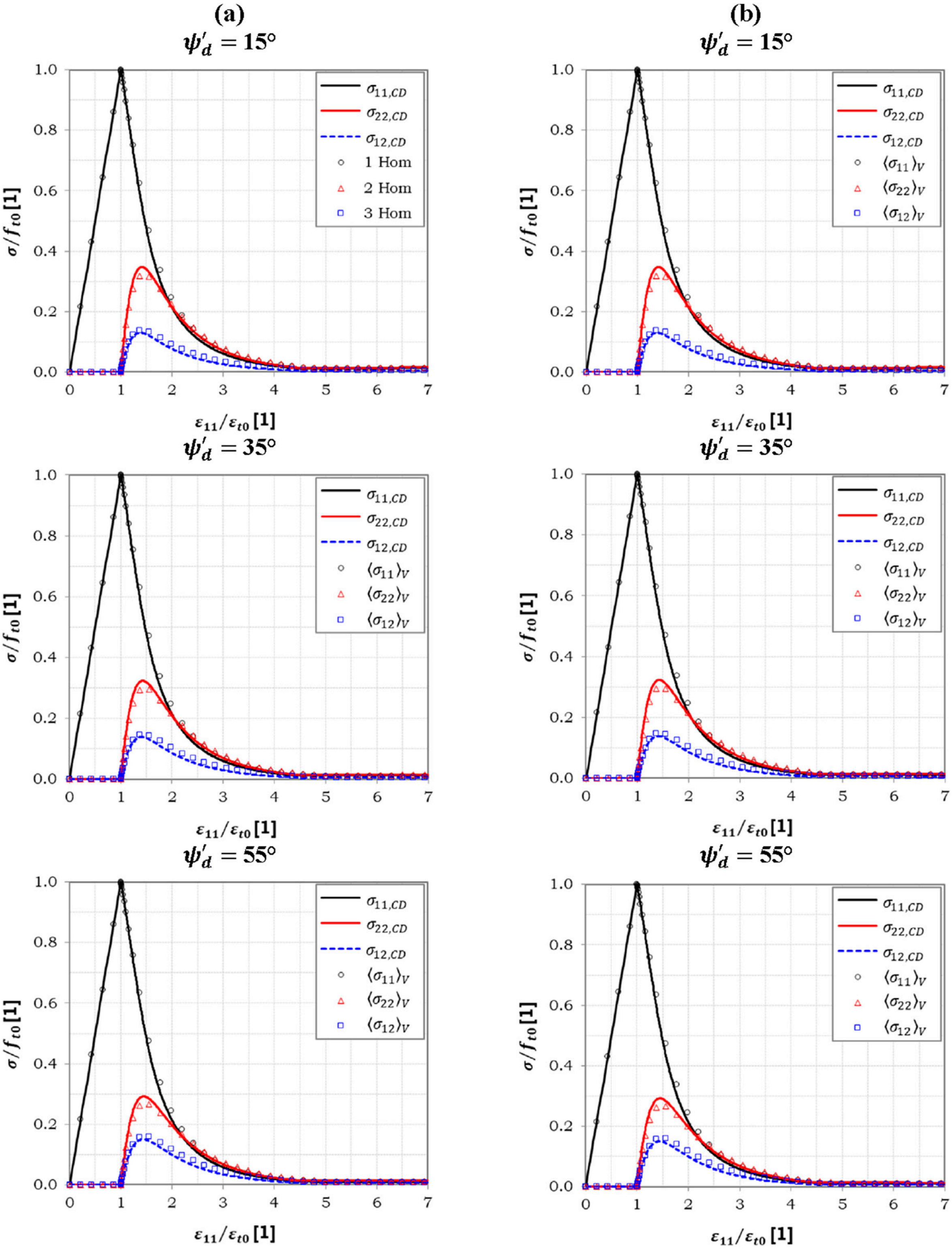

FIGURE 16
Comparison of stress components obtained from Willam's test at the constitutive-driver scale with those obtained at the specimen structural scale by homogenization in the absence of any imperfection for $\varepsilon_t^{ch} = 1{\cdot}10^{-4}$, $\alpha_p = 0.5$ and three values of dilatancy angle ψ'_d: **(a)** 8 × 8 mesh and **(b)** 32 × 32 mesh.

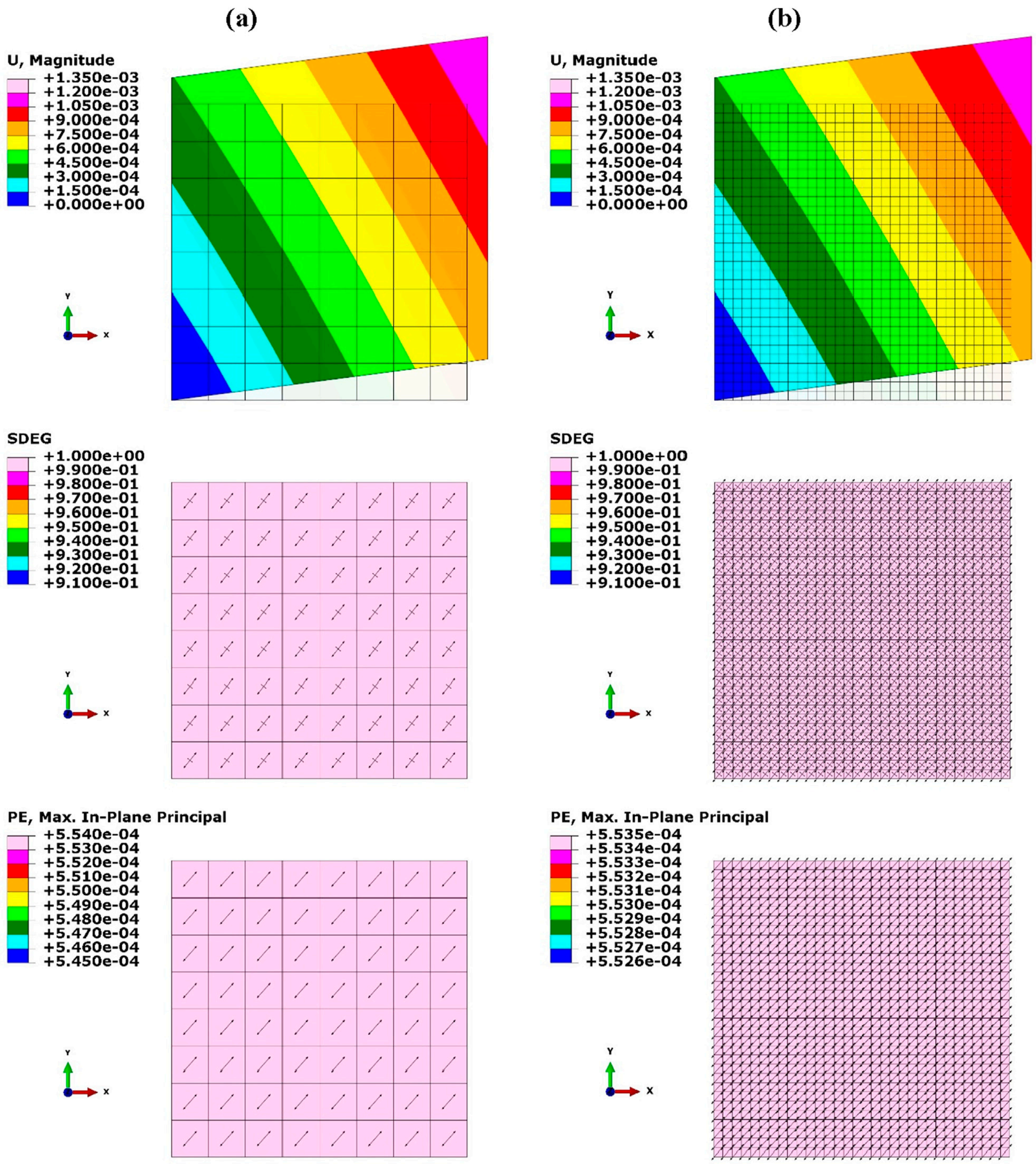

FIGURE 17
Maps of displacement magnitude (U), scalar damage variable (SDEG) with indication of principal stress directions and maximum principal plastic strain (PE) at the end of Willam's test ($\varepsilon_{11} = 8.5\varepsilon_{t0}$) in the absence of any imperfection for $\varepsilon_t^{ch} = 1{\cdot}10^{-4}$, $\alpha_p = 0.5$ and $\psi_d' = 35°$: **(a)** 8 × 8 mesh and **(b)** 32 × 32 mesh.

of elastoplastic coupling and correctly simulating tensile-dominated processes, with shearing, as per biaxial Willam's test, with extensive parametric analysis at the same local constitutive-driver scale of the resulting capabilities of the CDP model, and its "regularization" toward always ensuring "passing" Willam's test, in recording no residual stresses, in the progressive material annihilation, even at high plastic dilatancy.

c) Investigation of the constitutive structural scale, preluding subsequent real and wider structural scales, for the

10.3389/fmats.2026.1800938

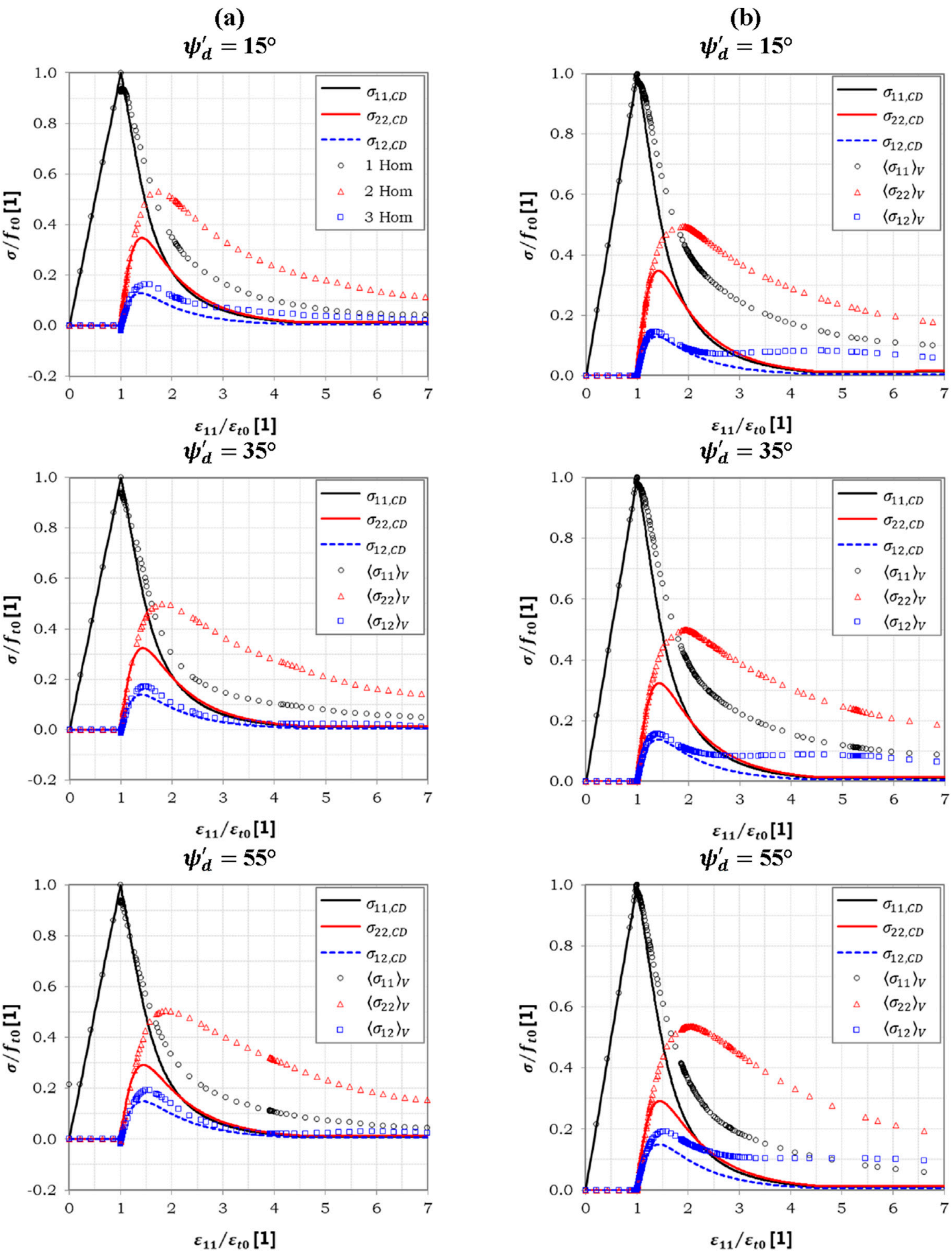

FIGURE 18
Comparison of stress components obtained from Willam's test at the constitutive-driver scale with those obtained at the specimen structural scale by homogenization with the considered imperfection for $\varepsilon_t^{ch} = 1{\cdot}10^{-4}$, $\alpha_p = 0.5$ and three values of dilatancy angle ψ_d': **(a)** 8 × 8 mesh and **(b)** 32 × 32 mesh.

10.3389/fmats.2026.1800938

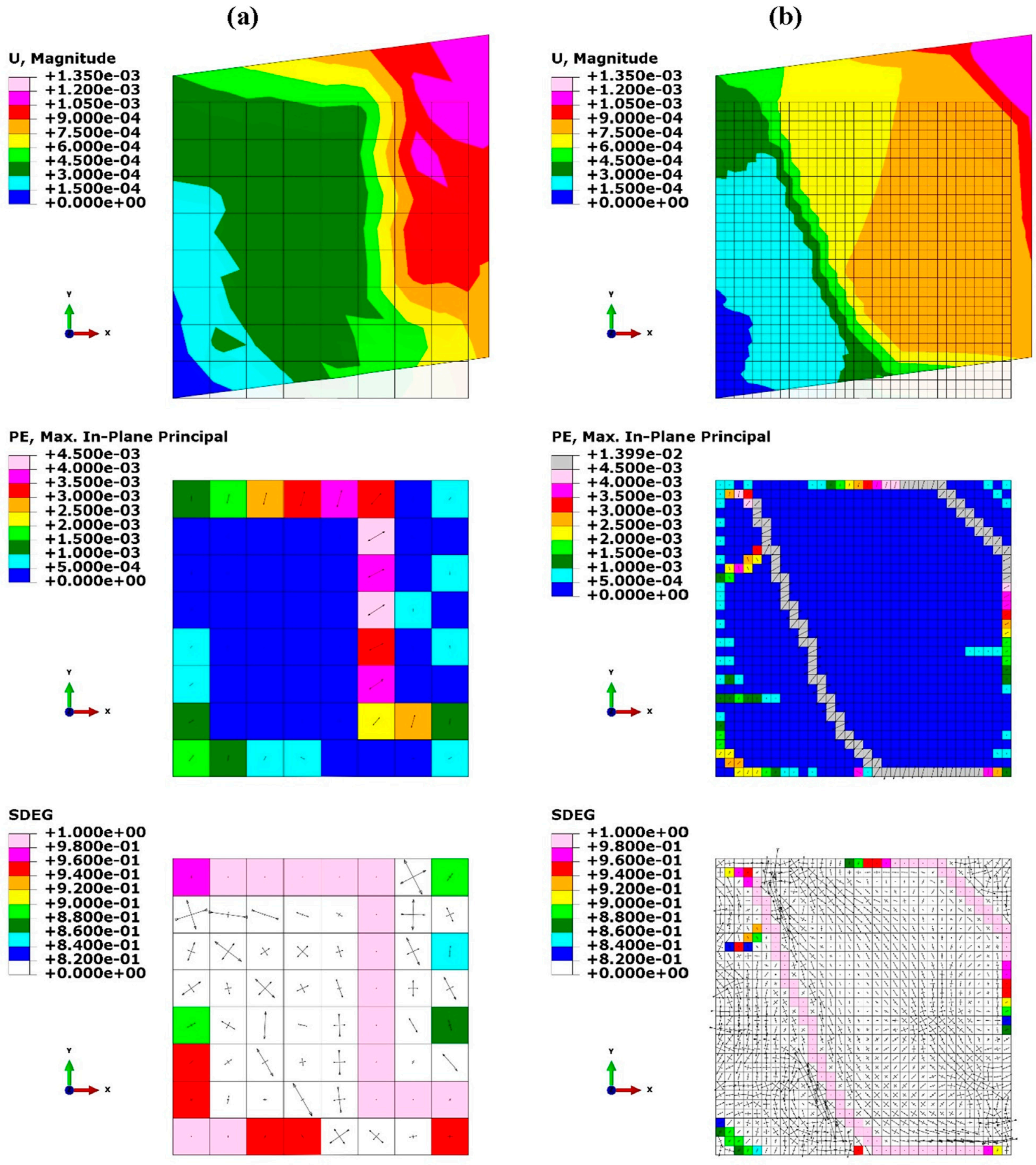

FIGURE 19
Maps of displacement magnitude (U), scalar damage variable (SDEG) with indication of principal stress directions and maximum principal plastic strain (PE) at the end of Willam's test ($\varepsilon_{11} = 8.5\varepsilon_{t0}$) with the considered imperfection for $\varepsilon_t^{ch} = 1{\cdot}10^{-4}$, $\alpha_p = 0.5$ and $\psi'_d = 35°$: **(a)** 8 × 8 mesh and **(b)** 32 × 32 mesh.

observation of inelastic-induced anisotropy, existence of residual stresses, and possible strain localization manifestation as perceived at the specimen size, as it may be described by the so-tuned CDP model.

As per first part a), the following main points and issues have been revealed:

- The conditions under which an anisotropic behavior may be predicted by the CDP model under multiaxial stress states have been investigated by an analysis of the constitutive equations of the material model, confirming that, as it may be expected, the only source of induced anisotropy at the local level shall arise from the development of plastic strains (strain-induced

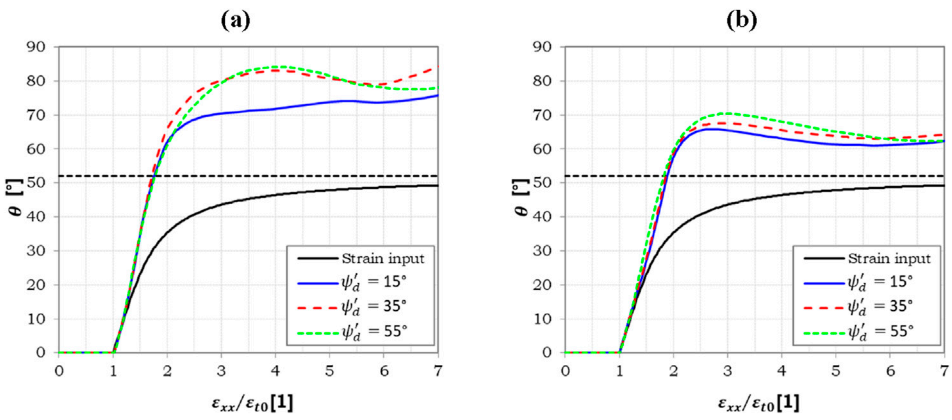

FIGURE 20
Imposed rotation of major principal strain axis and resulting rotation of major principal stress axis of the homogenized stress-strain fields at the structural scale under Willam's test ($\varepsilon_t^{ch} = 1 \cdot 10^{-4}$, $\alpha_p = 0.50$ and $\psi_d' = 35°$): **(a)** 8 × 8 mesh and **(b)** 32 × 32 mesh.

anisotropy), which also drive all the inelastic phenomena reproduced by the model (single-dissipative material, namely a single inelastic, i.e., plastic, multiplier describes the increments of the inelastic strains). Therein, plastic strain evolutions are ruled by effective stress path and by inherent plastic dilatancy.

- The theoretical formulation statements have been validated by extensive numerical simulations of the CDP model response to a peculiar non-radial loading path constituted by biaxial extension/shearing Willam's test. The analyses have been performed at a constitutive-driver level within ABAQUS, for a single square element, under displacement control.
- A consistent validation of the present CDP model check implementation has been achieved, based on numerical results of a couple of Willam's tests recently reported in (Wosatko et al., 2020), among the comparison of the performance of different constitutive models. The latter have been taken as a first benchmark reference, for the numerical solution, with rather close matches and commented relevant highlighted numerical and physical findings, which appear by themselves to be pretty interesting, for the interpretation of the CDP model capabilities, and limitations, as is.
- Indeed, excessive plastic dilatancy may considerably influence the resulting nonlinear response, specifically under biaxial (kinematically constrained) Willams' test, especially in the case of a plastic-dominated setting (exiguous damage), leading to "fail" the test, in terms of recordable non-zero (negative) residual stresses, an aspect that shall be regularized in the model description.

As per second part b), the following salient remarks may be listed:

- A comprehensive, easily reproducible, external parametrization of prescribed tensile post-peak strength exponential softening function $f_t(\varepsilon_I^i)$, depending on "brittleness" characteristic softening strain $\varepsilon_t^{ch} = g_t^f / f_{t0}$, as linked to the amount of specific fracture energy g_t^f, at given initial peak strength f_{t0}, and of attached tensile damage evolution function $D_t(\varepsilon_I^i)$, for tensile-dominated stress-strain states, has been proposed, by the introduction of a single suitable scalar material parameter, namely a plastic to inelastic strain ratio α_p, in the spirit of Ortiz's proposal (Ortiz, 1985), allowing to conveniently tune the amount of elastoplastic coupling, within the CDP model.
- Stress response curves, over imposed driving longitudinal strain, of both Cartesian and principal stress components have been traced, for various values of $\varepsilon_t^{ch} = g_t^f / f_{t0}$, of α_p, and of inherent CDP dilatancy angle ψ_d', taken as three free material parameters, the effects of which are aimed to be investigated, showing several important and characteristic features of the CDP constitutive response under biaxial Willam's test, namely:
    - Clearly, the material response to Willam's test is affected by the inherent amount of specific fracture energy, through variable ε_t^{ch}, with much enduring softening tails, at raising ε_t^{ch}.
    - The outcomes of Willam's test may result rather different, even if a source similar behavior in the uniaxial tension softening curve is scheduled, by varying the amount of elastoplastic coupling, through α_p.
    - Dilatancy angle ψ_d', instead, displays a rather minor effect on the stress response, except for the case in which plasticity is truly overriding stiffness degradation (slight or no damage, i.e., α_p approaching 1).
    - When plastic strains remain negligible overall (analyzed case of small $\alpha_p = 0.01$), though still driving the inelastic response, stress-strain axes co-rotate, independently of ψ_d'; however, once plastic strains are accounted for (analyzed mid-elastoplastic coupling case of $\alpha_p = 0.5$), plastic strain-induced anisotropy appears, so that stress increments come to over-rotate with respect to strain increments.
    - In the presence of stiffness degradation ($\alpha_p < 1$), damage eventually withdraws plastic strain-induced anisotropy at rather large strains, toward the tail of the softening range, so that material behavior returns to fully isotropic conditions, within the limit of very large strains.

As per third part c), the following core outcomes should be mentioned:

- The specimen response remains homogeneous, with confined inelastic-induced anisotropy, and self-coherent outfit, with the underlying material response, once no imperfections are present within the assumed FEM modelization of the kinematically controlled specimen under biaxial Willam's test.
- Strain localization and much higher inelastic-induced anisotropy arise, in the presence of (geometrical) imperfection, with rather rich features of resulting specimen response, specifically in terms of local stress-strain planar maps, nonlinear post-peak global softening description up to the tails of partial material annihilation and remarkable recorded over-rotation of principal stress directions to imposed strain directions, going beyond the imposed asymptotic rotation limit.
- This shows features that may be experienced from more sophisticated material models, as for instance anisotropic damage models [e.g. (Carol et al., 2001a); (Carol et al., 2001b); (Carol et al., 2008)], despite the intrinsic isotropic material description assumed within the CDP model, specifically in the damage part, of description of progressive stiffness degradation, still driven by plastic strains.
- This shows promise, for the further inspection of the potentialities of the so-tuned CDP model, in the analysis of large-scale concrete structures, still with a rather manageable and available constitutive model, accounting for elastoplastic coupling, at the continuum stress-strain scale (no need of describing macroscopic stress-displacement discontinuities, for instance by cohesive crack laws), at least for a first validation and load-bearing capacity inspection, toward design and safety assessment evaluation.

One may notice that the present study does not attempt a calibration of a specific material case. Instead, it investigates the range of performance behaviors of the material model through an enhanced tuning and extensive parametrization analysis. The achieved results shall turn out to be useful to researchers and practitioners involved in various practical applications of the so-tuned CDP model, specifically within numerical simulation environments. Along the same line, a quantitative analysis, experimental validation, or statistical evaluation are clearly out of the scope of the present investigation, which aims to offer a full panorama of the features that may be displayed by the CDP model in challenging loading contexts, such as that provided by multiaxial extension/shearing Willam's test.

Moreover, notice that the paper does not claim to propose a new model or FEM implementation. It aims to outline a research investigation able to address how to extract the best description capabilities, out of a known available model, on a given numerical platform. Toward that, an appropriate external tuning, and enhancing parametrization, is devised, as resumed in the pseudo-code chart in Table 1, which could become feasible, for an expert and keen user, willing to exploit the potentialities of an available platform not only as a plain black-box mechanical solver, to be independently reproduced by the information and results provided in the paper, to allow for complete and realistic simulations in the structural scale and scenario of specific engineering and research interest.

Further developments on investigating features and outcomes of the CDP model, for both theoretical and numerical scenarios, at the constitutive scale, in additional loading contexts, even in 3D scenarios, and possibly eventually at the practical structural scale, for instance for large-scale concrete structures, may further be investigated, as additional perspectives of the present study, in seeing up to where the available adoption of the CDP model may be pushed, for the expert and aware user, in handling real engineering applications, to achieve reasonable and affordable structural results, for informed judgement and management.

Data availability statement

The original contributions presented in the study are included in the article, further inquiries can be directed to the corresponding author.

Author contributions

DF: Conceptualization, Data curation, Formal Analysis, Investigation, Methodology, Resources, Software, Validation, Visualization, Writing – original draft, Writing – review and editing. RF: Funding acquisition, Supervision, Writing – review and editing, Project administration. ER: Conceptualization, Funding acquisition, Methodology, Project administration, Supervision, Validation, Visualization, Writing – original draft, Writing – review and editing.

Funding

The author(s) declared that financial support was received for this work and/or its publication. Financial support by the Italian Ministry of University and Research (MUR) under PRIN 2022 program (funding following reallocation of resources from the final ranking), Project Code 2022744YM9, CUP F53C24000930006 and by institutional research funds ("Fondi di Ricerca d'Ateneo ex 60%") at the University of Bergamo is gratefully acknowledged.

Conflict of interest

The author(s) declared that this work was conducted in the absence of any commercial or financial relationships that could be construed as a potential conflict of interest.

Generative AI statement

The author(s) declared that generative AI was not used in the creation of this manuscript.

Any alternative text (alt text) provided alongside figures in this article has been generated by Frontiers with the support of artificial intelligence and reasonable efforts have been made to ensure accuracy, including review by the authors wherever possible. If you identify any issues, please contact us.

Publisher's note

All claims expressed in this article are solely those of the authors and do not necessarily represent those of their affiliated organizations, or those of the publisher, the editors and the reviewers. Any product that may be evaluated in this article, or claim that may be made by its manufacturer, is not guaranteed or endorsed by the publisher.

References

ABAQUS (2025). *Version 2025*. USA: Dassault Systèmes Simulia Corp.

Bažant, Z. P. (1980). Work inequalities for plastic fracturing materials. *Int. J. Solids Struct.* 16 (10), 873–901. doi:10.1016/0020-7683(80)90055-4

Bažant, Z. P., and Oh, B. H. (1983). Crack band theory for fracture of concrete. *Matériaux Constr.* 16 (93), 155–177. doi:10.1007/bf02486267

Bažant, Z. P., and Planas, J. (1998). *Fracture and size effect in concrete and other quasibrittle materials*. London, UK: CRC Press.

Besson, J., Cailletaud, G., Chaboche, J.-L., and Forest, S. (2010). *Non-linear mechanics of materials*. Dordrecht, Netherlands: Springer Science+Business Media B.V.

Carol, I., Rizzi, E., and Willam, K. J. (2001a). On the formulation of anisotropic elastic degradation. I. Theory based on a pseudo-logarithmic damage tensor rate. *Int. J. Solids Struct.* 38 (4), 491–518. doi:10.1016/s0020-7683(00)00030-5

Carol, I., Rizzi, E., and Willam, K. J. (2001b). On the formulation of anisotropic elastic degradation. II. Generalized pseudo-Rankine model for tensile damage. *Int. J. Solids Struct.* 38 (4), 519–546. doi:10.1016/s0020-7683(00)00031-7

Carol, I., Rizzi, E., and Willam, K. J. (2008). Discussion on the paper: application of some anisotropic damage model to the prediction of failure of some complex industrial concrete structure, *Int. J. Solids Struct.*, 45(16), 4600–4602 [Badel P., Godard V., Leblond J.-B. (2007), International Journal of Solids and Structures, 44 (18-19), 5848–5874], doi:10.1016/j.ijsolstr.2008.03.021

Grassl, P., and Jirásek, M. (2006). Damage-plastic model for concrete failure. *Int. J. Solids Struct.* 43 (22-23), 7166–7196. doi:10.1016/j.ijsolstr.2006.06.032

Grassl, P., Nyström, U., Rempling, R., and Gylltoft, K. (2011). A damage-plasticity model for the dynamic failure of concrete, arXiv:1103.1288v2 [cond-mat.mtrl-sci] 8 Mar 2011, Proceedings of the 8th International Conference on Structural Dynamics, EURODYN 2011, Leuven, Belgium, 4-6 July 2011, G. De Roeck, G. Degrande, G. Lombaert, G. Müller Editors (Leuven, Belgium: Katholieke Universiteit Leuven), Paper MS22-1255, 8.

Grassl, P., Xenos, D., Nyström, U., Rempling, R., and Gylltoft, K. (2013). CDPM2: a damage-plasticity approach to modelling the failure of concrete. *Int. J. Solids Struct.* 50 (24), 3805–3816. doi:10.1016/j.ijsolstr.2013.07.008

Guzina, B., Rizzi, E., Willam, K., and Pak, R. Y. S. (1995). Failure predictions of smeared crack formulations. *J. Eng. Mech. (ASCE)* 121 (1), 150–161. doi:10.1061/(asce)0733-9399(1995)121:1(150)

Hueckel, T., and Maier, G. (1977). Incremental boundary value problems in the presence of coupling of elastic and plastic deformations: a rock mechanics oriented theory. *Int. J. Solids Struct.* 13 (1), l–15. doi:10.1016/0020-7683(77)90087-7

Lee, J., and Fenves, G. L. (1998). Plastic-damage model for cyclic loading of concrete structures. *J. Eng. Mech. (ASCE)* 124 (8), 892–900. doi:10.1061/(asce)0733-9399(1998)124:8(892)

Lubliner, J., Oliver, J., Oller, S., and Onate, E. (1989). A plastic-damage model for concrete. *Int. J. Solids Struct.* 25 (3), 299–326. doi:10.1016/0020-7683(89)90050-4

Maier, G., and Hueckel, T. (1979). Nonassociated and coupled flow-rules of elastoplasticity for rock-like materials. *Int. J. Rock Mech. Min. Sci.* 16 (2), 77–92. doi:10.1016/0148-9062(79)91445-1

Mehta, P. K., and Monteiro, P. J. M. (2006). *Concrete: microstructure, properties, and materials*. 3rd Ed. New York, USA: McGraw-Hill.

Meschke, G., Macht, J., and Lackner, R. (1998). A damage-plasticity model for concrete accounting for fracture-induced anisotropy. In: H. Mang, N. Bićanić, and R. de Borst Editors *Computational Modelling of Concrete Structures*, Balkema, Badgastein, Austria; pp. 3–12.

Ogden, R. W. (1997). *Non-linear elastic deformations*. Mineola, New York (USA): Dover Publications Inc.

Oliver, J., Cervera, M., Oller, S., and Lubliner, J. (1990). Isotropic damage models and smeared crack analysis of concrete. *Computer-Aided Analysis and Design of Concrete Structures, vol 2*. Editors N. Bićanić, and H. Mang (Austria: Pineridge, Zell-am-See), 945–957.

Oller, S., Oñate, E., Oliver, J., and Lubliner, J. (1990). Finite element nonlinear analysis of concrete structures using a "plastic-damage model". *Eng. Fract. Mech.* 35 (l/2/3), 219–231. doi:10.1016/0013-7944(90)90200-z

Ortiz, M. (1985). A constitutive theory for the inelastic behavior of concrete. *Mech. Mater.* 4 (1), 67–93. doi:10.1016/0167-6636(85)90007-9

Pramono, E., and Willam, K. (1989). Fracture energy-based plasticity formulation of plain concrete. *J. Eng. Mech. (ASCE)* 115 (6), 1183–1203. doi:10.1061/(asce)0733-9399(1989)115:6(1183)

Rizzi, E., Maier, G., and Willam, K. (1996). On failure indicators in multi-dissipative materials. *Int. J. Solids Struct.* 33 (20-22), 3187–3214. doi:10.1016/0020-7683(95)00247-2

Rots, J. G. (1988). *Computational modelling of concrete fracture*. Ph.D. thesis. Delft, Netherlands: Delft University of Technology, 141.

Willam, K., Pramono, E., and Sture, S. (1987). Fundamental issues of smeared crack models. In: *Proceedings of SEM/RILEM International Conference of Fracture and Rocks; Houston, Texas (USA), June 17–19*. Editors S. P. Shah, and S. E. Swartz. Berlin, Germany: Springer, 142–157.

Wosatko, A., Szczecina, M., and Winnicki, A. (2020). Selected concrete models studied using Willam's test. *Materials* 13 (21), 4756–4779. doi:10.3390/ma13214756

Xotta, G., Beizaee, S., and Willam, K. J. (2016). Bifurcation investigations of coupled damage-plasticity models for concrete materials. *Comput. Methods Appl. Mech. Eng.* 298 (2016), 428–452. doi:10.1016/j.cma.2015.10.010

Yu, X., Chang, H., Jin, H., Linforth, S., Wang, P., Chen, A., et al. (2025a). Peridynamic modelling of concrete under impact loading: a critical review of theories, models, applications, and challenges. *Int. J. Impact Eng.* 206 (December 2025), 105457. doi:10.1016/j.ijimpeng.2025.105457

Yu, X., Chen, A., and Chang, H. (2025b). Simulating concrete cracking and failure under impact loading using a novel constitutive integration paradigm in non-ordinary state-based peridynamics. *Eng. Fract. Mech.* 314 (2025), 110703. doi:10.1016/j.engfracmech.2024.110703

Zienkiewicz, O. C., Taylor, R. L., and Zhu, J. Z. (2013). *The finite element method: its basis and fundamentals*. 7th Ed. Oxford, UK: Elsevier.